NAVAL POSTGRADUATE SCHOOL

MONTEREY, CALIFORNIA

THESIS

MULTI-HYPERSONIC MISSILE TARGET SELECTION AND TRAJECTORY OPTIMIZATION

by

Michael L. Zepeda

December 2023

Thesis Advisor:	Mark Karpenko
Second Reader:	Jeffery T. King

THIS PAGE INTENTIONALLY LEFT BLANK

REPORT DOCUMENTATION PAGE	*Form Approved OMB No. 0704-0188*

1. AGENCY USE ONLY ***(Leave blank)***	**2. REPORT DATE** December 2023	**3. REPORT TYPE AND DATES COVERED** Master's thesis

4. TITLE AND SUBTITLE
MULTI-HYPERSONIC MISSILE TARGET SELECTION AND TRAJECTORY OPTIMIZATION

5. FUNDING NUMBERS

6. AUTHOR(S) Michael L. Zepeda

7. PERFORMING ORGANIZATION NAME(S) AND ADDRESS(ES)
Naval Postgraduate School
Monterey, CA 93943-5000

8. PERFORMING ORGANIZATION REPORT NUMBER

9. SPONSORING / MONITORING AGENCY NAME(S) AND ADDRESS(ES)
Joint Hypersonic Transition Office, Crane, In 47522

10. SPONSORING / MONITORING AGENCY REPORT NUMBER

11. SUPPLEMENTARY NOTES The views expressed in this thesis are those of the author and do not reflect the official policy or position of the Department of Defense or the U.S. Government.

12a. DISTRIBUTION / AVAILABILITY STATEMENT
Approved for public release. Distribution is unlimited.

12b. DISTRIBUTION CODE
A

13. ABSTRACT (maximum 200 words)

Current approaches to performing target selection optimization with trajectory optimization is through enumeration of the different trajectories and then performing a binary target selection optimization on the constructed cost matrix. Issues with this method are that the target selection problem requires up to n! calculations, and that each of these calculations is performed devoid of information of the other agents and can therefore result in collisions when applied to missile flight profiles. Being able to solve the assignment problem concurrently with the trajectory optimization is of interest in solving multi-hypersonic missile trajectories because of the potential saving of computational time as well as solving the issue of collision avoidance. This thesis seeks to develop and solve the bi-level optimization problem of a multi-hypersonic missile target selection problem by embedding the target selection optimization inside a trajectory optimization loop using a "Designer Function." This maps the XOR statement of a target selection problem into a continuous conjunctive setup. This allows the problem to be solved simultaneously for which asset goes to which target without telling the system a specific missile-target pairing. Analysis of DIDO solutions using Pontryagin's Principle verifies that this method produces an optimal result in a 2 x 2 scenario.

14. SUBJECT TERMS Pontryagin's Principle; trajectory optimization; costate; DIDO; Hamiltonian; Lagrangian; optimal control	**15. NUMBER OF PAGES** 95
	16. PRICE CODE

17. SECURITY CLASSIFICATION OF REPORT	**18. SECURITY CLASSIFICATION OF THIS PAGE**	**19. SECURITY CLASSIFICATION OF ABSTRACT**	**20. LIMITATION OF ABSTRACT**
Unclassified	Unclassified	Unclassified	UU

NSN 7540-01-280-5500

Standard Form 298 (Rev. 2-89)
Prescribed by ANSI Std. 239-18

THIS PAGE INTENTIONALLY LEFT BLANK

Approved for public release. Distribution is unlimited.

MULTI-HYPERSONIC MISSILE TARGET SELECTION AND TRAJECTORY OPTIMIZATION

Michael L. Zepeda
Lieutenant, United States Navy
BA, Thomas Aquinas College, 2011
BS, University of North Dakota, 2016

Submitted in partial fulfillment of the
requirements for the degree of

MASTER OF SCIENCE IN ASTRONAUTICAL ENGINEERING

from the

NAVAL POSTGRADUATE SCHOOL
December 2023

Approved by: Mark Karpenko
Advisor

Jeffery T. King
Second Reader

Brian S. Bingham
Chair, Department of Mechanical and Aerospace Engineering

THIS PAGE INTENTIONALLY LEFT BLANK

ABSTRACT

Current approaches to performing target selection optimization with trajectory optimization is through enumeration of the different trajectories and then performing a binary target selection optimization on the constructed cost matrix. Issues with this method are that the target selection problem requires up to n! calculations, and that each of these calculations is performed devoid of information of the other agents and can therefore result in collisions when applied to missile flight profiles. Being able to solve the assignment problem concurrently with the trajectory optimization is of interest in solving multi-hypersonic missile trajectories because of the potential saving of computational time as well as solving the issue of collision avoidance. This thesis seeks to develop and solve the bi-level optimization problem of a multi-hypersonic missile target selection problem by embedding the target selection optimization inside a trajectory optimization loop using a "Designer Function." This maps the XOR statement of a target selection problem into a continuous conjunctive setup. This allows the problem to be solved simultaneously for which asset goes to which target without telling the system a specific missile-target pairing. Analysis of DIDO solutions using Pontryagin's Principle verifies that this method produces an optimal result in a 2 x 2 scenario.

THIS PAGE INTENTIONALLY LEFT BLANK

Table of Contents

List of Figures

THIS PAGE INTENTIONALLY LEFT BLANK

List of Tables

THIS PAGE INTENTIONALLY LEFT BLANK

List of Acronyms and Abbreviations

DOD	Department of Defense
HGV	Hypersonic Glide Vehicle
HMC	Hamiltonian minimization condition
HVC	Hamiltonian value condition
KKT	Karush-Kuhn-Tucker
LSAP	Linear Sum Assignment Problem
NPS	Naval Postgraduate School
OCP	Optimal Control Problem
USN	U.S. Navy
WTA	Weapon-Target Assignment Problem

THIS PAGE INTENTIONALLY LEFT BLANK

Acknowledgments

I would like to thank my advisor Dr. Mark Karpenko for putting up with my math errors and reading my rough drafts that feel and sound like a bull in a china shop. Somehow, despite it all, the problems were fixed and my lack of writing skills has been overcome.

I would also like to thank my children. While my studies have had me learn about space and rockets, they are the real stars in my eyes.

And finally I would like to thank my wife Bridget. You have always pushed me to follow my dreams and try to reach my full potential. Despite the late nights, the "I don't know when I'll be home today," the spending more time in my office then ever, and the editing my "math with no numbers," you still pushed, supported, and encouraged me to finish this journey of being a "rocket scientist."

THIS PAGE INTENTIONALLY LEFT BLANK

CHAPTER 1:
Introduction

1.1 Motivation

In multi-agent scenarios involving different desired end goals for each agent, solving the assignment problem is difficult and time consuming. When the assignment problem is that of "What missile or munition goes to which target in order to achieve the optimal outcome?" it is referred to as a Weapon-Target Assignment Problem (WTA). Numerous works on optimizing the solution to WTA have been written over the years [1]–[4].

However, these works focus on the assignment problem specifically as the probability of kill/survival (P_k) and do not consider the assignment according to a trajectory optimization, which in and of itself can affect the P_k. Injecting the calculus of optimizing the trajectory of the weapon changes this problem from being a classical WTA since the problem can no longer be considered a static optimization problem, and must now be solved as a dynamic trajectory optimization problem to account for the dynamic constraints of the weapon over the time history of the engagement.

The probability of kill of a Hypersonic Glide Vehicle (HGV) is dependent on the trajectory that it takes to reach its target. The reason for this is two-fold. The first is that the nature of HGV's system dynamics make them incredibly sensitive to the flight conditions on the trajectory to the target. The extreme speeds of Mach 5.0+ makes slight changes in control inputs and flight path trajectories result in significant effects on the aerodynamic loads as well as on the aerodynamic heating. This sensitive nature of the HGV affects the P_k of the HGV by just the fact of whether it makes it too the target or not. The second reason is that the probability of the adversary detecting the HGV is dependent on how long the missile is in the detection envelope. The possibility to either intercept or disable the weapon through EM or IR counter measures is dependent on the path the missile takes as well as the flight conditions of the missile. Because of this it is crucial to perform trajectory optimization of the HGV.

Little literature exists for co-operative trajectory optimization for an attack on a single target, and even less on engaging multiple targets simultaneously via optimal trajectories. Many works seek to only apply a target selection optimization for multi-missile multi-target scenarios through the use of genetic algorithms [5] or a particle swarm algorithm [6]. These methodologies do not perform trajectory optimization for the weapons and presuppose the existence of an assignment cost matrix for each missile target assignment. Co-operative missile optimization for a shared target has been investigated using sequential convex methods [7], and feasibility of multi-missile systems through a cooperative consensus control law [8]. However these methods assume the predetermined assignment or that the missiles all have the same target and that no selection process is required.

1.1.1 Overview of US Hypersonic Missiles

A hypersonic missile is a missile that is capable of flying/gliding and maneuvering at velocities of Mach 5.0+. Current research and development is being done in multiple countries, causing an arms race to occur in developed nations [9]. Hypersonic missiles can be broken down into two types: a hypersonic cruise missile that produces thrust through advanced scramjet technology, or a hypersonic-glide vehicle (HGV) that is launched like a conventional ballistic missile with the upper stage being the HGV that glides at hypersonic speeds to its target while maneuvering in the upper atmosphere to direct its trajectory. A major advantage to this form of weaponry compared to ballistic missiles is both the reduced time to detect the missile at the target site as well as the maneuverability of the missile makes it difficult to accurately predict what the missile is targeting. Figure 1.1 shows a graphic illustrating the flight path difference between the hypersonic missile types.

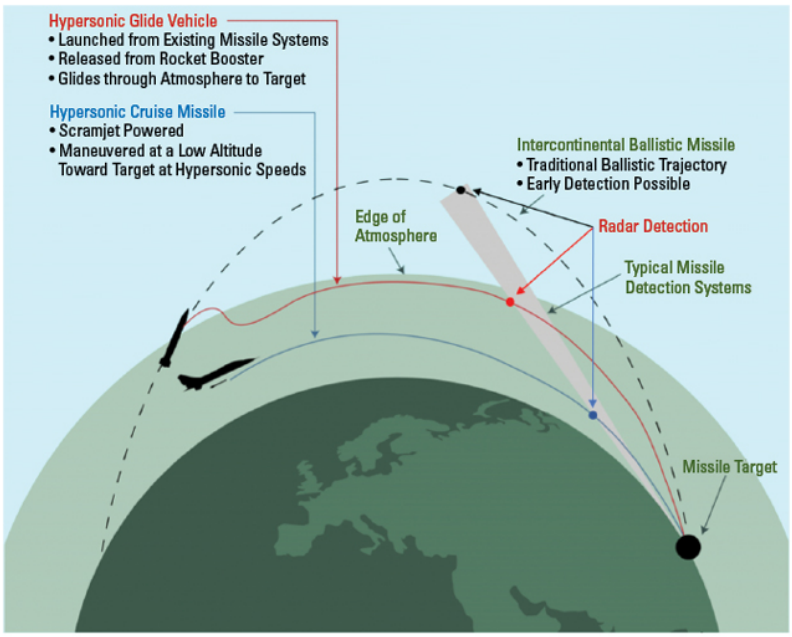

Figure 1.1. Flight Path Comparisons Between Intercontinental Ballistic Missile, Hypersonic Cruise Missile, and Hypersonic Glide Vehicle. Source: [10].

The US Navy and the Army are co-developing a Common-Hypersonic Glide Body for both forces future use. The HGV body is based on the research of Sandia National Laboratories Alternate Reentry Vehicle research that was done in the 70s and 80s [11]. The booster missile with the attached hypersonic glide body is referred to as the All-Up-Round (AUR) [12], which is common to both services, Figure 1.2. The Army was scheduled to start fielding its canister version of the AUR in September 2023 [13], but has been delayed out past FY2023 [12]. The Navy plans to implement its canister version of the AUR on the Zumwalt class destroyer in FY 2025 and on the Block V Virginia class submarine in FY2028 [14].

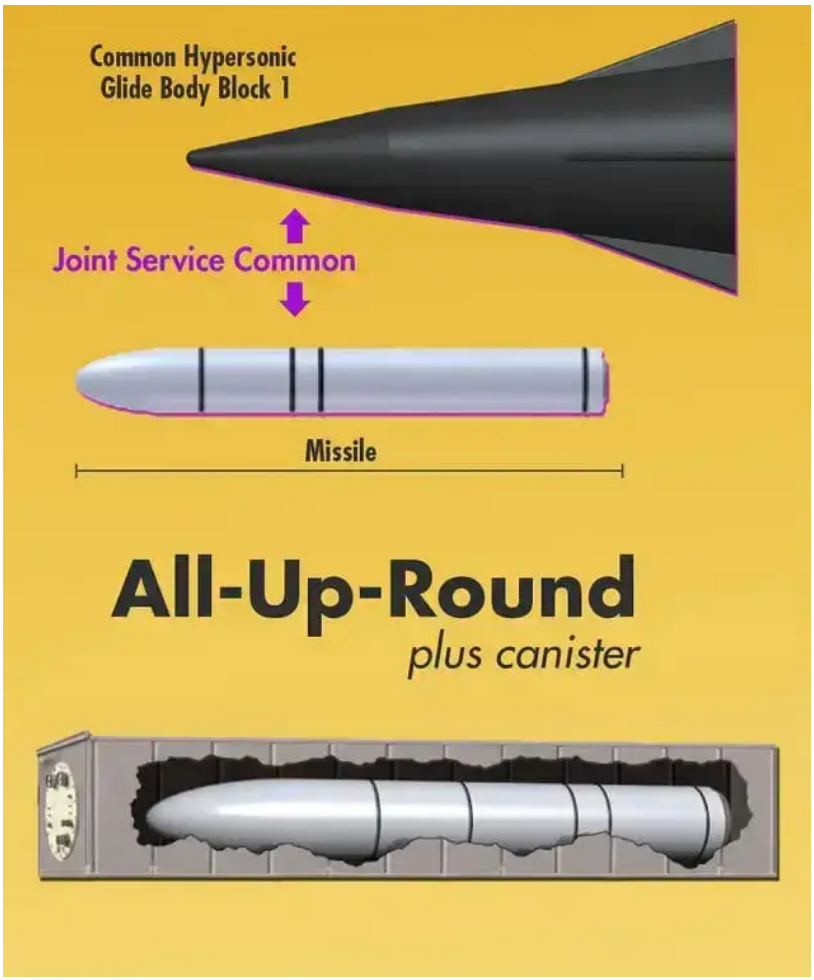

Figure 1.2. Common Hypersonic Glide Body with the Booster Missile. Source: [15].

The implementation of swarm tactics with hypersonic missiles through the use of multiple missiles being used in tandem will greatly increase the effectiveness of hypersonic missile strikes. With the high speeds and maneuverability of hypersonics an adversary has little time to detect and react to a hypersonic missile threat. Firing multiple HGVs to fly in unison on multiple targets takes further advantage of an adversary's inability to adequately counter-act the hypersonic threat by increasing the number of threats that need to be tracked and responded to.

The Department of Defense does not plan on utilizing hypersonics for nuclear strikes [14],

rather they are to be used for conventional strikes. A conventional strike requires that the HGV have a precise and accurate trajectory in order to ensure successful utilization of the warhead onto the intended target. With there being multiple hypersonics and targets, a target selection problem also needs to be solved along with the trajectory optimization.

1.2 Thesis Objective and Scope

This thesis presents several different methods to solve a minimum time, simultaneous time-of-arrival hypersonic glide missile target selection and trajectory optimization problem. These strategies result in either missile collisions or not arriving at the same time. This prevents methods from being used in a simultaneous time-of-arrival setup. A solution to the collision issue while ensuring simultaneous time-of-arrival is through the use of a baseline system-of-systems approach. This methodology requires that an inner-loop and outer-loop architecture to be used to ultimately solve the target selection problem. The reason for this is due to the nature of the missile-target pairing being exclusive. This creates a discrete XOR scenario for the unique missile-target pairings. A solution to the issues of collisions and time-of-arrival differences as well as the problem of solving discrete XOR requirements in a continuous algebra is then presented through the use of problem specific constraint mappings of the disparate endpoints to a continuous curve. This converts the XOR endpoint statements of the assignment problem into a Boolean And statement.

The scope of this thesis focuses primarily on how the XOR solution can be ultimately converted into a collection of AND statements, solving the assignment problem while also not falling into the issues that sequential methodologies possess. Therefore, without loss of generality a simple drag model of the hypersonics missiles can be utilized with the missiles constrained to lie only on the cross and downrange positions. The results of this methodology can be applied in future works to more detailed models and HGV simulation.

1.3 Thesis Outline

This thesis introduces an HGV multi-missile target selection and minimum time of flight trajectory optimization problem for a final flight corridor entering at different locations. Chapter 2 details what is meant by trajectory optimization and the necessary mathematical requirements that need to be met in order to have an optimal solution. Chapter 3 applies

the theory of optimality to solving an intuitive based enumeration approach to solving a target selection and trajectory optimization of HGVs. This chapter highlights the pitfalls and issues that arise in attempting such an enumeration methodology. Chapter 4 expands on the enumeration method from Chapter 3's approach, using a missile hierarchy to attempt to circumvent a missile collision problem. However, this in turn raises a complication of the missiles not arriving at the same time. Chapter 5 creates a system of missiles problem that resolves the collision issue while maintaining simultaneous time-of-arrival, creating a valid baseline of trajectories but still being an enumeration method. Chapter 6 illustrates how to write a disjunctive logic of *XOR* as a set of Boolean *AND*s and solve the time Optimal Control Problem (OCP) with no user selection of missile-target assignments. Finally, Chapter 7 outlines the conclusions of this work, as well as presents considerations for future follow-on work to this thesis.

CHAPTER 2:
Pontryagin's Minimization Principle

A problem common to almost all technical fields is that of solving the OCP. These sorts of problems are asking what is the required control input to complete the trajectory with the minimum amount of system cost. In physical trajectories, e.g. flight path of a missile, the intuitive approach would be to follow a straight path between the initial and final point. However, due to the non-linear nature that exists in real world specific problems and the complicated coupling between the dynamics, system and component level constraints, and the control input, the optimal solution is rarely a straight line. Ross defines the OCP as, "a standard optimal control problem can be defined in terms of finding a dynamically feasible state-control function pair, $\mathbf{x}(\cdot)$, $\mathbf{u}(\cdot)$, that transfers the state system, $x \in \mathbb{R}^{N_x}$, from a given initial condition, $\mathbf{X}(t_0) = \mathbf{x}^0$, to a target condition $\mathbf{e}(\mathbf{x}_f, t_f) = 0$, while minimizing a given cost functional, $\mathbf{J}$" [16]. The specifics of an individual problem's setup dictates the specific solution to the OCP. Irrespective of the details, the standard description of a continuous-time-optimal control problem is given as [16]:

$$
\begin{aligned}
&\left.\begin{aligned}
&\boldsymbol{x} \in \mathbb{R}^{N_x} = (x_1, \ldots, x_{N_x}) \qquad \boldsymbol{u} \in \mathbb{R}^{N_u} = (u_1, \ldots, u_{N_u})
\end{aligned}\right\} \text{(preamble)} \\
&\textit{OCP:}\begin{cases}
\text{Minimize} \quad J[\boldsymbol{x}(\cdot), \boldsymbol{u}(\cdot), t_0, t_f] := \\
\qquad\qquad E(\boldsymbol{x}_0, \boldsymbol{x}_f, t_0, t_f) + \displaystyle\int_{t_0}^{t_f} F(\boldsymbol{x}(t), \boldsymbol{u}(t), t)\, dt \quad \Big\} \text{(cost)} \\
\text{Subject to} \qquad \dot{\boldsymbol{x}} = \boldsymbol{f}(\boldsymbol{x}(t), \boldsymbol{u}(t), t) \quad \Big\} \text{(dynamics} := \mathcal{D}) \\
\qquad\qquad \boldsymbol{e}^L \leq \boldsymbol{e}(\boldsymbol{x}_0, \boldsymbol{x}_f, t_0, t_f) \leq \boldsymbol{e}^U \quad \Big\} \text{(events} := \mathcal{E}) \\
\qquad\qquad \boldsymbol{h}^L \leq \boldsymbol{h}(\boldsymbol{x}(t), \boldsymbol{u}(t), t) \leq \boldsymbol{h}^U \quad \Big\} \text{(path} := \mathcal{H})
\end{cases}
\end{aligned}
$$

The cost functional J is the summation of the Mayer cost E, and the integral of the running cost F over the control problem's time horizon. The inputs to this functional are the state variables ($\mathbf{x}$), time (t), and the control inputs ($\mathbf{u}$).

The objective of this problem is to solve/find the minimum state control function pairing $t \rightarrow (\mathbf{x}, \mathbf{u})$ that minimizes the cost J. In solving the problem the differential equations that model the physical dynamics of the system ($\mathcal{D}$), the constraints placed upon the trajectory path and control inputs ($\mathcal{H}$) and the end-point event conditions ($\mathcal{E}$) must all be satisfied simultaneously. These constraints must be solved as logical conjunctions (see [17] for a discussion on the logical connectives). VonWeller points out this implies that "[T]he logical expression $\mathcal{D} \wedge \mathcal{E} \wedge \mathcal{H}$ must be true for a feasible solution" [18].

The proof that a problem statement has an optimal solution is a non-trivial problem. Currently only a small subset of problem types can be proven to possess an OCP solution [19]. However, if an optimal solution exists for an OCP then Pontryagin's Principle provides the necessary conditions that establish the optimality of a candidate solution. The conditions are listed as Theorem 2.1 in Ross's book:

> **Theorem 2.1 (Pontryagin's Principle)** Given an optimal solution to Problem B, there exists an absolutely continuous covector function $\boldsymbol{\lambda}(\cdot)$ and a covector $\boldsymbol{\nu}$ that satisfy
>
> - the three Hamiltonian conditions:
> 1. Hamiltonian minimization condition,
> 2. Hamiltonian value condition,
> 3. Hamiltonian evolution equation,
> - the adjoint equations, and
> - the transversality condition. [16]

Even though the proof that an optimal solution exists for a particular problem might not be currently solved, it is assumed that if a feasible solution exists then at least one optimal solution exists for the OCP, with the added assumption that the OCP is properly formulated, (see [16] for proper problem formulation). If there is a feasible solution that satisfies the logical connective $\mathcal{D} \wedge \mathcal{E} \wedge \mathcal{H}$ as well as meets the conditions of Pontryagin's Principle, then it is considered optimal if it has the lowest solution value for the cost functional J.

DIDO [20] is a MATLAB based toolbox that can be used to solve OCPs. A common issue for all gradient based solver algorithms is that they can get stuck in a local minima in the

solution space. This cannot be entirely avoided for OCPs that do not have an analytical closed form solution. To address this challenge DIDO monitors of the Lyapunov function of the search trajectory which acts akin to a momentum term in its solver algorithm to help prevent the solution from getting trapped in a local minima [20]. This idea of using a gradient based search with momentum is widely used in machine learning to help prevent entrapment in local minima and achieve better results [21]. It is important to note that this does not prevent solutions from becoming trapped in local minima, only aids in getting closer to the global optima. This ability to still get stuck in local minima is ultimately due to the a numeric based solutions only approximating the continuous solution space down to machine epsilon.

Another major advantage of using DIDO for solutions is that it does not require a user based guess to find a solution [22]. This means that solutions that are generated form DIDO are not because of a "lucky" guess from the user.

THIS PAGE INTENTIONALLY LEFT BLANK

CHAPTER 3:
Sequential Solutions for the Target Assignment

In Chapter 2 the OCP was defined as set of conjunctively true statements of problem dynamics ($\mathcal{D}$), endpoint events ($\mathcal{E}$) and path constraints ($\mathcal{H}$). However, in a HGV target selection problem the endpoint events are no longer a logical expression exclusively of *AND* statements. For example, let there be a set of missiles 1, 2, and 3 with possible targets A, B, and C. Each missile-target pairing creates for that missile a logical OR statement between that pairing and the other possible pairings since a missile can obviously only go to one target. Since each target in this scenario must be hit, the missiles are also exclusive in their target selection, converting the logical OR of each missile-target pairing into a discrete XOR statement. This means that the logical expression in the OCP is no longer conjunctively true. The intuitive thought for how to solve this disjunction in $\mathcal{E}$ is to solve the problem sequentially over all the possible combinations. Effectively this is turning the single target selection problem into a series of conjunctively true problems, which would then be solved for the optimal solution.

This chapter investigates the first attempt at solving this HGV target-trajectory problem through this enumeration method, which is effectively an inner and outer loop problem solution. This concept of inner-loop and outer-loop architecture has been used to optimize many astrodynamical problems [23] [24]. The inner loop sequentially solves each HGV independently for a missile-target pair, of which each solution cost to the missile-target pair is an entry, c_{ij} in the target selection cost matrix C. The outer loop would then solve the for the least total sum cost of the possible combinations of missile-target pairings. The mathematical modeling of the outer loops problem can be written as:

$$\min \quad \sum_{i=1}^{n} \sum_{j=1}^{n} c_{i\,j} x_{i\,j}, \tag{3.1}$$

$$\text{s.t.} \quad \sum_{i=1}^{n} x_{i\,j} = 1, \tag{3.2}$$

$$\text{s.t.} \quad \sum_{j=1}^{n} x_{i\,j} = 1, \tag{3.3}$$

$$x_{ij} \in \{0,\ 1\}, \tag{3.4}$$

with $X = x_{i\,j}$ being the permutation matrix of the missile-target pairings. This problem is referred to as Linear Sum Assignment Problem (LSAP) or sometimes the Worker Assignment problem (see [25] for a more in depth explanation of the LSAP).

3.1 Problem Formulation

A two dimensional layout of the HGV target selection problem can be seen in Figure 3.1. Each HGV is entering the final flight corridor from a different angle to simulate the HGVs either having different launch locations or having made previous maneuvers to avoid possible detection or interception. The HGV pair is required to take out the pair of targets A and B simultaneously, minimizing the final time for missile strike. For the problem formulation the two missiles are assumed to have similar physical profiles for ease in the solving of the problem formulation through symmetry. This would not be the case for a real system and would just require that the coefficients of the dynamics to be adjusted accordingly to provide a higher fidelity model, but the general solution analysis that is provided in this and later chapters is still valid. It must be noted that it is common in solving OCPs that proper scaling and balancing of the problem parameters into canonical units to reduce the required parameters to solve the problem. Throughout this thesis canonical units will be used for distance, time etc. unless explicitly stated otherwise.

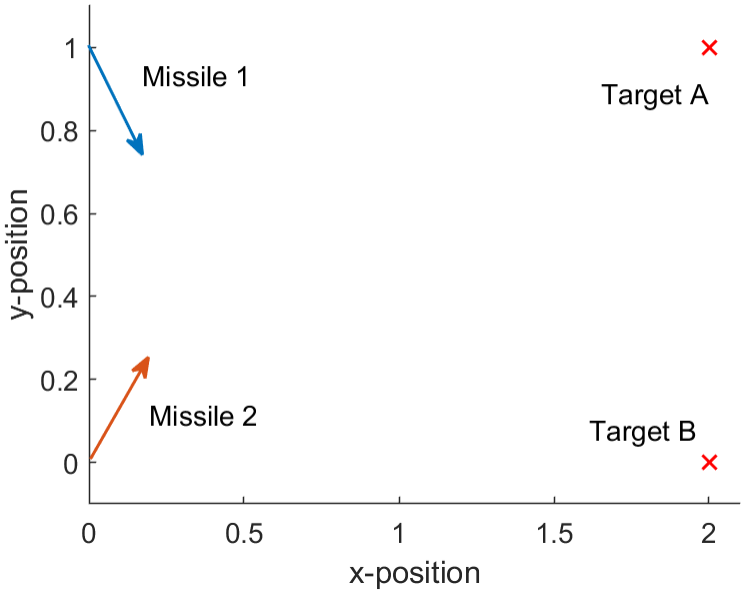

Figure 3.1. Initial Hypersonic Glide Vehicle Target Scenario

The HGV dynamics and boundary conditions for this 2×2-DOF problem are modeled as

$$\textit{HGV Dynamics} \begin{cases} \dot{x} = V cos\theta \\ \dot{y} = V sin\theta \\ \dot{V} = -(k_1 + k_2\omega^2)V^2 \\ \dot{\theta} = \omega \end{cases} \qquad \textit{Boundary Conditions} \begin{cases} x_0, y_0 = HGV_1^0 \vee HGV_2^0 \\ V_0, \theta_0 = (c, \pm d) \\ x_f, y_f = A \vee B \\ V_f, \theta_f = \text{free} \end{cases}.$$

The state variables for this are

$$\mathbf{x} = \begin{bmatrix} x \\ y \\ V \\ \theta \end{bmatrix},$$

with the control being the angular turn rate ω that would be induced by the control surfaces of the HGV. If constraints are to be placed on the final speed and angle of impact then V_f and θ_f would have values, however since no constraint is placed upon them, in this problem they are free.

Putting this into the OCP formulation, each missile-target scenario can be written as,

$$\mathbf{x}^T := [x, y, V, \theta] \in \mathbb{R}^4, \quad \mathbf{u} := \omega \in \mathbb{R} : |\omega| \leq \omega_{max}$$

$$HGV_i \text{ to } Target\ P \begin{cases} \text{Minimize} & J[\mathbf{x}(\cdot), \mathbf{u}(\cdot), t_f] = & t_f \\ \text{Subject to} & \dot{x} = & V cos\theta \\ & \dot{y} = & V sin\theta \\ & \dot{V} = & -(k_1 + k_2\omega^2)V^2 \\ & \dot{\theta} = & \omega \\ & V(t_0) = & V_0 \\ & t_0 = & 0 \\ & \mathbf{x}_0 = & (HGV_i(t_0), c, \pm d) \\ & e_1(\mathbf{x}_f) = & x_f - P_x = 0 \\ & e_2(\mathbf{x}_f) = & y_f - P_y = 0 \end{cases} \tag{3.5}$$

with parameter values in Table 3.1.

Table 3.1. Problem Data

Parameter	Value
$HGV_1(t_0)$	(0, a)
$HGV_2(t_0)$	(0, 0)
A	(b, a)
B	(b, 0)
a	1
b	2
c	1
d	1.22 rad
k_1	0.5
k_2	0.15
ω_{min}	-1.4 rad/TU
ω_{max}	1.4 rad/TU

For the setup in problem Equation (3.5), the enumeration can be broken down into two cases for the missile-target scenario:

Case 1:	Case 2:
Missile 1 goes to Target A,	Missile 1 goes to Target B,
Missile 2 goes to Target B.	Missile 2 goes to Target A.

3.1.1 Establishing the Necessary Conditions

In order to show that the solutions to the HGV target assignment problem is optimal, the necessary conditions for optimality for problem 3.5 must be constructed. The first step is to construct the Hamiltonian according to

$$H = F + \boldsymbol{\lambda}^T f(\mathbf{x}, \mathbf{u}, t). \tag{3.6}$$

The first term, F, is the running cost of the problem, and represents the integrated term of the cost-function J. There is no running cost in this problem, so F goes to 0. The second term is the costate vector dotted with the HGV Dynamics $\mathcal{D}$. Since the dynamics of both missiles are identical each missile has the same Hamiltonian form,

$$H = \lambda_x V cos(\theta) + \lambda_y V sin(\theta) - \lambda_V (k_1 + k_2 \omega^2) V^2 + \lambda_\theta \omega \tag{3.7}$$

The addition of the constraints on the minimum and maximum control were accounted for by taking the Lagrangian of the Hamiltonian ($\bar{H}$), equation (3.8), as seen in Equation (3.9).

$$\bar{H} = H + \boldsymbol{\mu}^T h(\mathbf{x}, \mathbf{u}) \tag{3.8}$$

$$\bar{H} = \lambda_x V cos(\theta) + \lambda_y V sin(\theta) - \lambda_V (k_1 + k_2 \omega^2) V^2 + \lambda_\theta \omega + \mu\omega \tag{3.9}$$

The value of the covariable, μ, is given by the Karush-Kuhn-Tucker (KKT) conditions,

$$\mu \quad \begin{cases} \leq 0, & \text{if} \quad \omega = \omega_{\min}, \\ = 0, & \text{if} \quad \omega_{\min} < \omega < \omega_{\max}, \\ \geq 0, & \text{if} \quad \omega = \omega_{\max} \end{cases} \tag{3.10}$$

From Equation (3.10) it is apparent that the value of the covariable μ is only nonzero when

the control is at either a maximum or a minimum. So while the KKT conditions do not give values for the covariables at the control extremes, they do allow checking the sign of μ in order to verify the validity of the generated solution..

Minimizing $\bar{H}$ with respect to the control ω, (the stationarity condition), also provides information how the control input over the time history must behave for an optimal trajectory solution.

$$\frac{\partial \bar{H}}{\partial \mathbf{u}} = 0 \tag{3.11}$$

$$-2\lambda_V k_2 \omega V^2 + \lambda_\theta + \mu = 0 \tag{3.12}$$

The adjoint equations developed with,

$$-\dot{\boldsymbol{\lambda}} = \frac{\partial \bar{H}}{\partial \mathbf{x}} \tag{3.13}$$

give information on the costates behavior over the problem time history for an optimal trajectory solution. In this case, the costates can be seen to be,

$$-\dot{\lambda}_x = 0 \quad \rightarrow \quad \lambda_x = \text{constant} \tag{3.14}$$

$$-\dot{\lambda}_y = 0 \quad \rightarrow \quad \lambda_y = \text{constant} \tag{3.15}$$

$$-\dot{\lambda}_V = \lambda_x cos\theta + \lambda_y sin\theta - 2\lambda_V(k_1 + k_2\omega^2)V \tag{3.16}$$

$$-\dot{\lambda}_\theta = -\lambda_x V sin\theta + \lambda_y V cos\theta \tag{3.17}$$

The next step in verifying optimality is through the construction of the Endpoint Lagrangian ($\bar{E}$) according to,

$$\bar{E} = E + \boldsymbol{\nu}^T \boldsymbol{e}(\boldsymbol{x}_f). \tag{3.18}$$

For the current problem formulation ($\bar{E}$) is,

$$\bar{E} = t_f + \nu_1(x_f - P_x) + \nu_2(y_f - P_y). \tag{3.19}$$

The Hamiltonian Value Condition was used as seen in Equation (3.20) to analyze the value of the Hamiltonian at t_f,with the result given in Equation (3.21).

$$\bar{H}(t_f) = -\frac{\partial \bar{E}}{\partial t_f} \tag{3.20}$$

$$\bar{H}(t_f) = -1 \tag{3.21}$$

The Hamiltonian evolution is shown in Equation (3.22). Since there is no explicit dependence on t in the Lagrangian of the Hamiltonian, the value of the Lagrangian of the Hamiltonian is constant except for allowed jump discontinuities from the μ terms according to the KKT conditions.

$$\frac{dH}{dt} = \frac{\partial \bar{H}}{\partial t} = 0 \tag{3.22}$$

The final value of the costates can be seen in Equation(3.23)-(3.26). The unknown values of ν_1 and ν_2 give no meaningful information on λ_x and λ_y. However, useful information is provided for λ_V and λ_θ, namely both $\lambda_V(t_f)$ and $\lambda_\theta(t_f)$ equal 0.

$$\boldsymbol{\lambda}_x(t_f) = \nu_1 \tag{3.23}$$

$$\boldsymbol{\lambda}_y(t_f) = \nu_2 \tag{3.24}$$

$$\boldsymbol{\lambda}_V(t_f) = 0 \tag{3.25}$$

$$\boldsymbol{\lambda}_\theta(t_f) = 0 \tag{3.26}$$

In addition to providing the necessary conditions for optimality, Pontryagin's Principle also supplies the necessary information to solve the problem statement. Looking at the boundary conditions for the problem it can be seen that only six of the eight required boundary values are given for the 4 state problem. The additional information given by the Terminal Transversality of the Endpoint Lagrangian provides the missing two pieces of boundary conditions to solve the BVP, namely $\lambda_V(t_f) = 0$ and $\lambda_\theta(t_f) = 0$. In addition to these boundary conditions the Hamiltonian value condition, Equation (3.21), provided the additional information for the added unknown variable of t_f.

3.1.2 Solutions and Verification of Case 1

Comparing the DIDO solutions to the conditions for optimality and the boundary conditions for the HGVs in case 1 determines if they can be called optimal. The boundary conditions

for missile 1 in case 1 are,

$$\begin{aligned} x_1(0) &= 0; \quad y_1(0) = a; \quad v_1(0) = c; \quad \theta_1(0) = -d; \\ x_1(t_f) &= b; \quad y_1(t_f) = a; \quad \lambda_{v1}(t_f) = 0; \quad \lambda_{\theta 1}(t_f) = 0. \end{aligned} \tag{3.27}$$

and the boundary conditions for missile 2 in case 1 are,

$$\begin{aligned} x_2(0) &= 0; \quad y_2(0) = 0; \quad v_2(0) = c; \quad \theta_2(0) = d; \\ x_2(t_f) &= b; \quad y_2(t_f) = 0; \quad \lambda_{v2}(t_f) = 0; \quad \lambda_{\theta 2}(t_f) = 0. \end{aligned} \tag{3.28}$$

The generated solution met the boundary conditions for the states and control of missile 1 as can be seen in Figure 3.2. The minimized t_f for missile 1 in case 1 was 2.90 normalized time units.

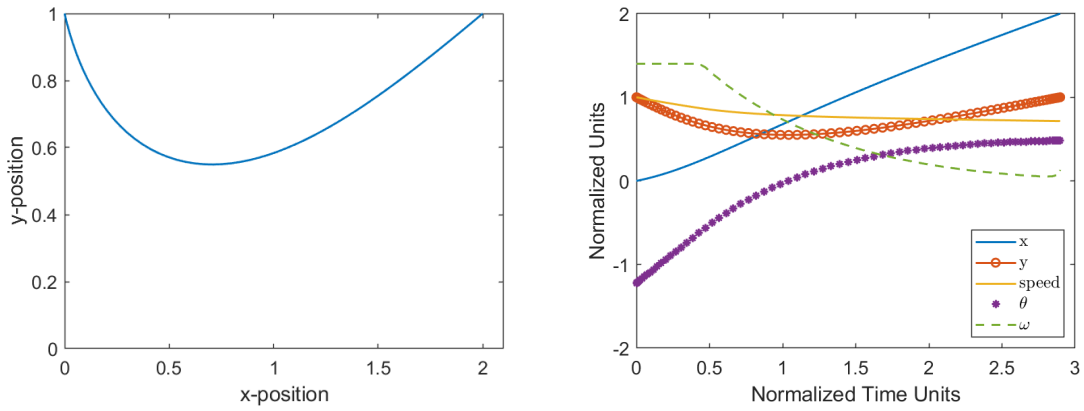

(a) (b)

Figure 3.2. Missile 1 to Target A (a) Trajectory (b) States and Control Input

The requirements of the adjoint Equations (3.14-3.17) are met when compared to Figure 3.3a. Costates λ_x and λ_y are constant, while the remaining costates have behavior that is consistent with theory. The terminal transversality Equations (3.23-3.26) are also met in the generated solution with $\lambda_V(t_f)$ and $\lambda_\theta(t_f)$ meeting tolerance levels of 0 at $\lambda_V(t_f) = -1.0 \times 10^{-3}$ and $\lambda_\theta(t_f) = 1.23 \times 10^{-5}$.

The Hamiltonian evolution and Hamiltonian minimization condition (HMC) are met as can

be seen in Figure 3.3b. The Hamiltonian shows a constant $H(t) = -1$ value over the entire time history of the generated solution. The control history of missile 1 in Figure 3.3c shows that the control input is at ω_{max} for the first 0.5 time units. The covariable μ shows an activation during this time period in accordance with the KKT conditions, Equation (3.10), going back to 0 at 0.52 time units when the control variable comes of the bounds of the path constraint.

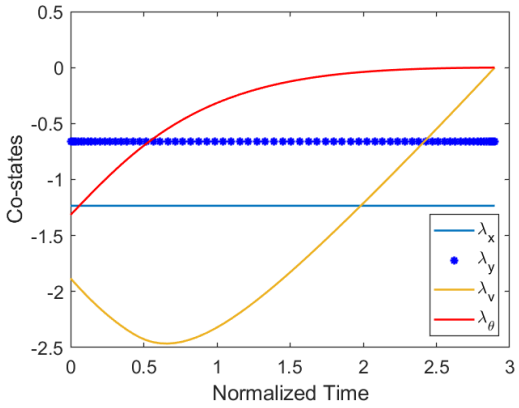

(a)

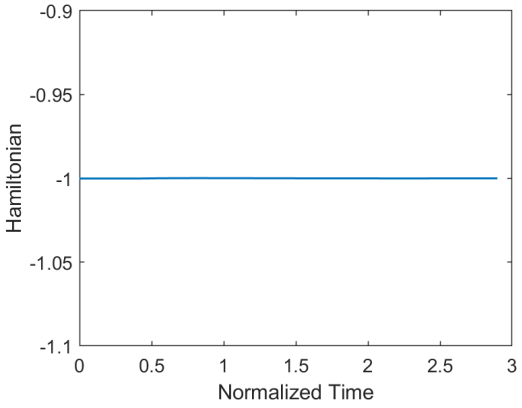

(b)

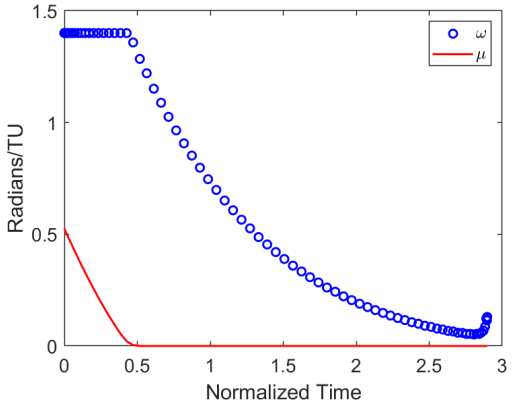

(c)

Figure 3.3. Missile 1 to Target A (a) Costates (b) Hamiltonian (c) Control and Covector μ.

The generated solution for case 1 met the boundary conditions for the states and control of missile 2 as can be seen in Figure 3.4. The minimized t_f for missile 2 in case 1 was 2.90 normalized time units, the same value as missile 1. Comparing both the trajectory and

the history of states and control of missile 2 with those of missile 1 shows a mirroring of the trajectories. This is to be expected due to the symmetrical problem setup, and further demonstrates that the generated solutions are valid according to the problem formulation.

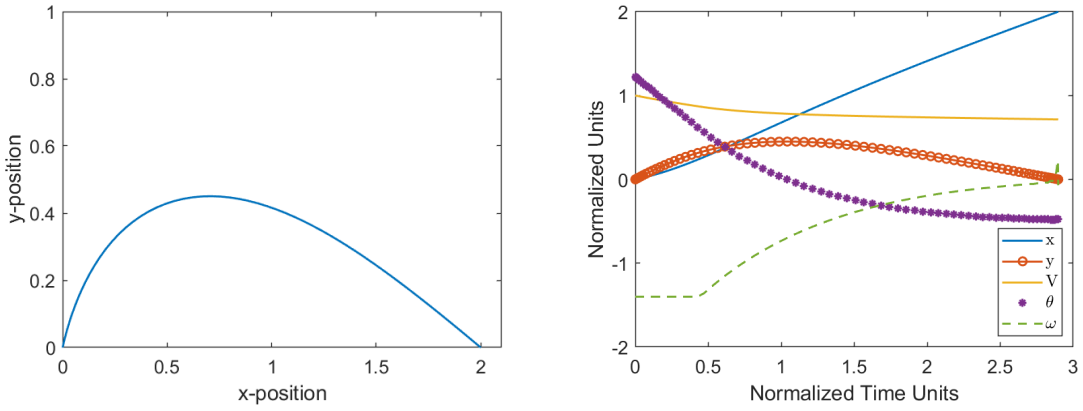

(a) (b)

Figure 3.4. Missile 2 to Target B (a) Trajectory (b) States and Control Input.

Just as for missile 1 in case 1, the adjoint equations were properly satisfied, as well as the terminal transversality equations when compared to the generated solution seen in Figure 3.5a. The values of $\lambda_V(t_f)$ and $\lambda_\theta(t_f)$ both got within acceptable tolerance levels of 0 with $\lambda_V(t_f) = -1.0 \times 10^{-3}$ and $\lambda_\theta(t_f) = 1.63 \times 10^{-5}$ for missile 2. The HMC and the Hamiltonian evolution were also met with a constant $H(t) = -1$ value throughout the trajectory solution's time history, Figure 3.5b. The KKT conditions were met, with missile 2 mirroring the solutions of missile 1 for the control and covariable values, Figure 3.5c.

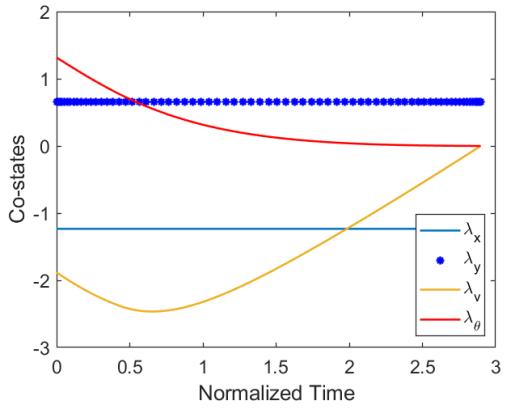

(a)

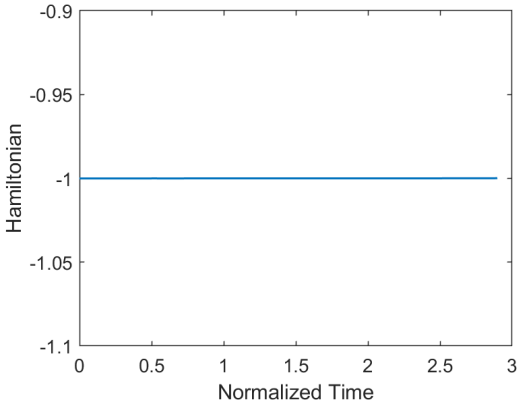

(b)

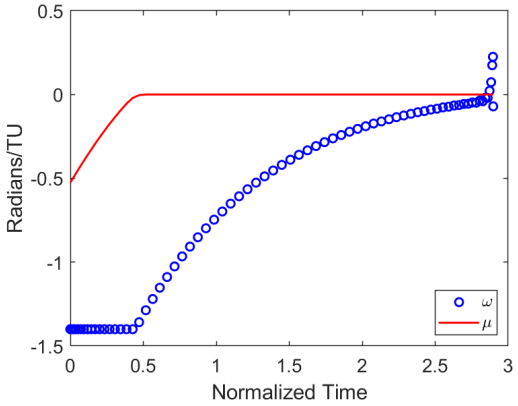

(c)

Figure 3.5. Missile 2 to Target B (a) Costates (b)Hamiltonian (c) Control and Covector μ

From this analysis it can be concluded that the generated trajectories are optimal for both HGVs in case 1.

3.1.3 Solutions and Verification of Case 2

The same analysis needs to be repeated for case 2 when the missile-target pairings are switched so that missile 1 goes to target B and missile 2 goes to target A. The boundary

conditions for missile1 in case 2 are,

$$\begin{aligned} x_1(0) &= 0; \quad y_1(0) = a; \quad v_1(0) = c; \quad \theta_1(0) = -d; \\ x_1(t_f) &= b; \quad y_1(t_f) = 0; \quad \lambda_{v1}(t_f) = 0; \quad \lambda_{\theta 1}(t_f) = 0. \end{aligned} \tag{3.29}$$

And the boundary conditions for missile 2 in case 2 are,

$$\begin{aligned} x_2(0) &= 0; \quad y_2(0) = 0; \quad v_2(0) = c; \quad \theta_2(0) = d; \\ x_2(t_f) &= b; \quad y_2(t_f) = a; \quad \lambda_{v2}(t_f) = 0; \quad \lambda_{\theta 2}(t_f) = 0. \end{aligned} \tag{3.30}$$

The generated solution met the boundary conditions for the states and control of missile 1 as can be seen in Figure 3.6. The minimized t_f for missile 1 in case 2 was 2.69 normalized time units.

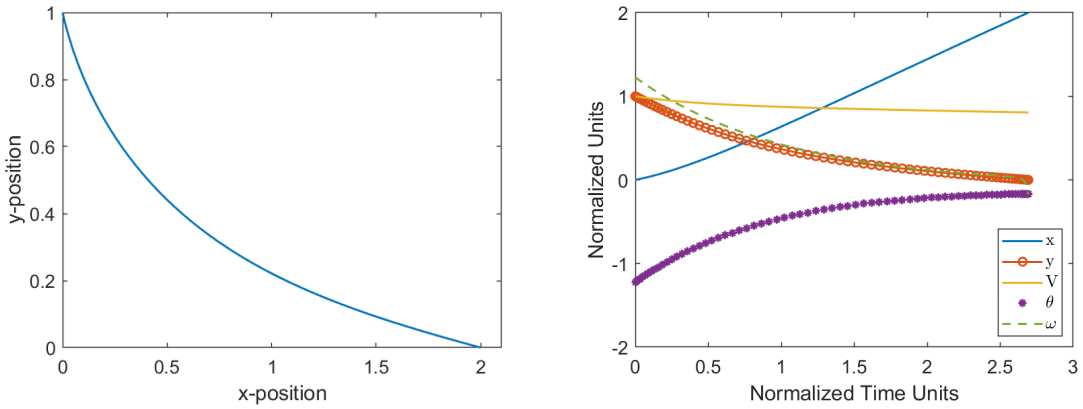

(a) (b)

Figure 3.6. Missile 1 to Target B (a) Trajectory (b) States and Control Input

The generated solution for missile 2 also met the boundary conditions for the state and control as can be seen in Figure 3.7. The same t_f of 2.69 was the optimized time for missile 2.

The adjoint equations, HMC and Hamiltonian evolution, and the KKT conditions for the covariable μ are met for missile 1 as seen in Figure 3.8. No activation of μ occurred since the control input never met a minimum or maximum allowed value.

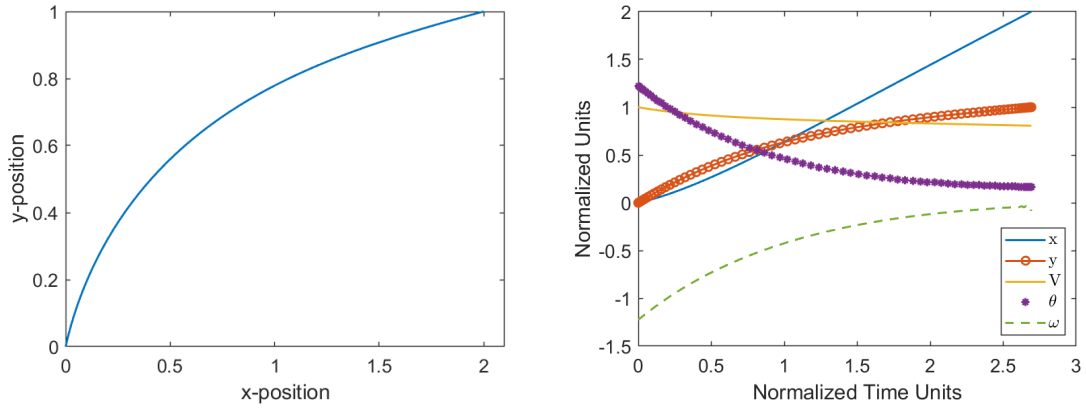

(a) (b)

Figure 3.7. Missile 2 to Target A (a) Trajectory (b) States and Control Input

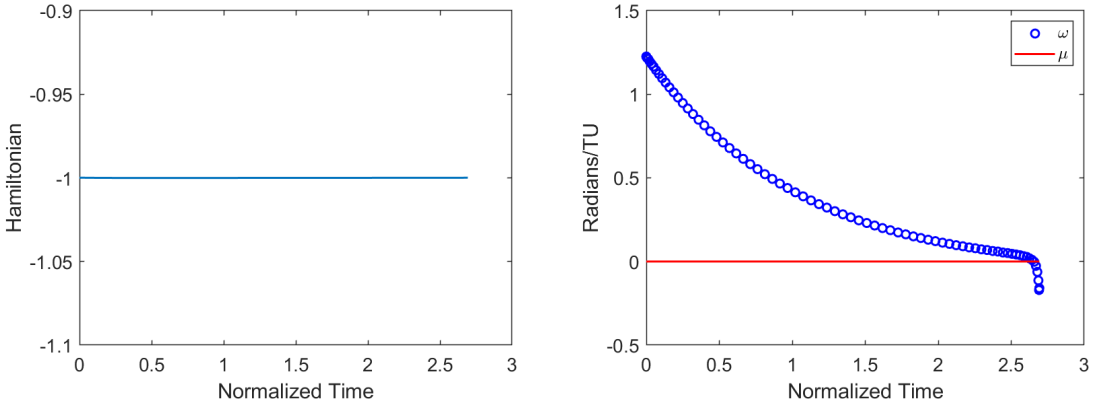

(a) (b)

Figure 3.8. Missile 1 to Target B (a) Costates (b)Hamiltonian (c) Control and Covector μ

Likewise the adjoint equations, HMC and Hamiltonian evolution, and the KKT conditions are met for missile 2 as seen in Figure 3.9.

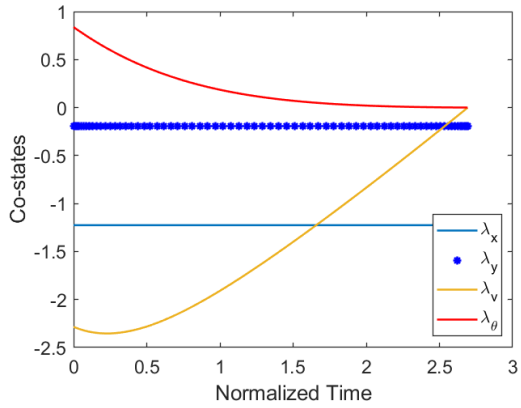

(a)

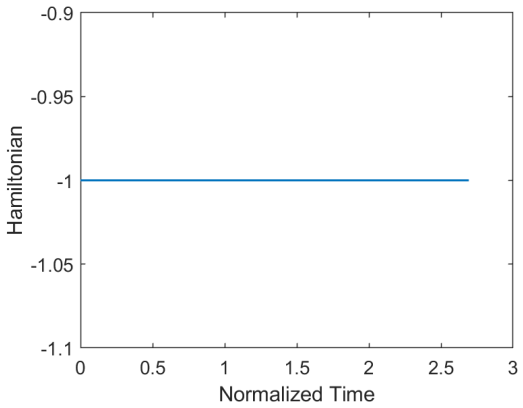

(b)

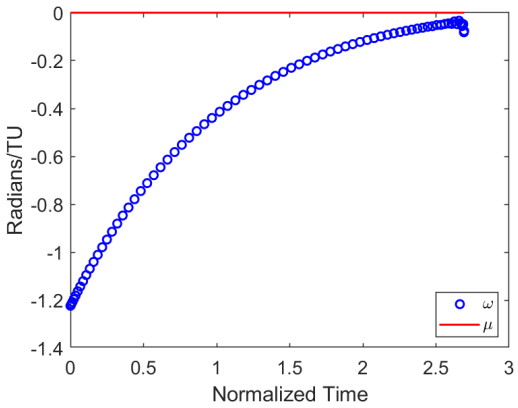

(c)

Figure 3.9. Missile 2 to Target A (a) Costates (b) Hamiltonian (c) Control and Covector μ

From this it can be concluded that according to the problem formulation the solved trajectories for case 2 are optimal for both missiles.

3.2 Cost and Trajectory Analysis

Constructing the cost matrix from the individual costs from the two cases gives

$$\mathbf{C} = \begin{bmatrix} 2.90 & 2.69 \\ 2.69 & 2.90 \end{bmatrix}. \tag{3.31}$$

The rows of this matrix represent the missiles, with missile 1 being the top row and missile 2 being the bottom row. The columns are from left to right, target A and Target B. Each entry in the cost matrix is the associated cost for the corresponding missile-target pairing. Since this is a simple 2x2 cost matrix a simple comparison of the main and counter diagonal is required. From this it can be seen that the scenario with the fastest time to target is case 2 where missile 1 goes to target B and missile 2 goes to target A. In a larger system the target assignment problem would have a larger cost matrix that can not be solved by a simple investigation of the diagonals. Instead it would need to be solved with a computationally expensive algorithm for solving LSAPs, (reference [25] for an in depth look at different methods of assignment problems and their solutions). An example of how to solve a simple 4x4 cost matrix using the basic $O(n^4)$ Hungarian method can be seen in [26].

The solution to case 1 gives a time to target time of $t_f = 2.90$ while case 2 gives a time to target time of $t_f = 2.69$, a difference of 0.21 in normalized time units. An explanation of why this is the case can be seen by looking at the trajectories of both missiles for case 1 versus case 2 in Figure 3.10. It can be seen that in case 1 the HGVs require a larger control input in order to be able to turn to their intended target. Since this problem models the drag loss that would occur in turning a missile, more velocity is lost in case 1 with the final velocities of the missiles being 0.715 canonical speed units in versus 0.806 canonical speed units in case 2.

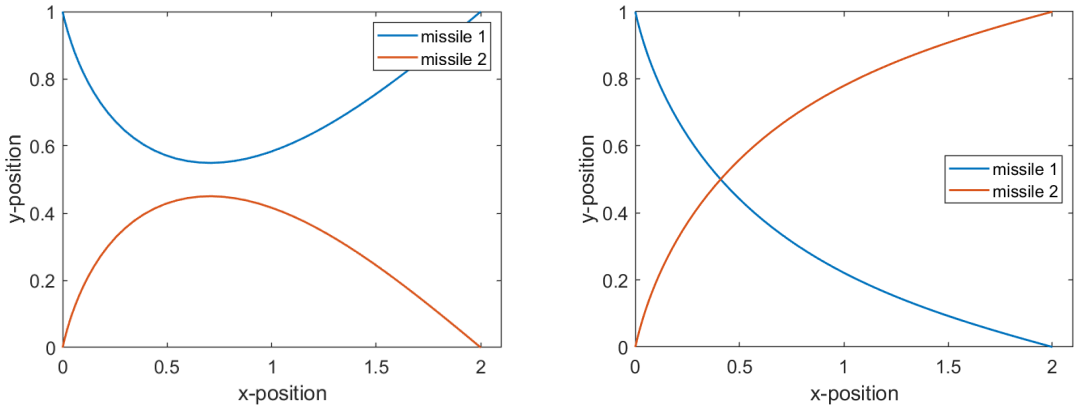

(a) Case 1 (b) Case 2

Figure 3.10. Combined HGV Trajectories

This suggests that case 2 is the better target assignment. However, investigating the trajectories of the missiles for the two cases demonstrates an issue with this simple enumeration method. Looking closer at both missiles' trajectories in case 2 one sees that they cross paths. The crossing of the missiles actually leads to a collision at $t = 0.712$. which invalidates the analysis of this being the target assignment for minimum time to target.

3.3 Chapter Summary

The simple enumeration of the OCP to bypass the discrete nature of XOR does not actually work in providing a means to find the optimal target selection and trajectory optimization for the HGVs. With the construction of the OCP it is possible that the missiles collide in flight, invalidating the corresponding trajectory solution. To even check for feasible solutions for the HGV-target pairing collision checks have to performed between the missiles. This scenario of collisions gets even worse if one were to expand the system since the missile interactions that must be considered for possible collisions is $(n-1)!$. From this it can be concluded that a different method of enumeration must be considered to find the optimal trajectory solutions to even use in an LSAP for the outer loop architecture.

CHAPTER 4:
Lead and Follow-on Missile Solutions

It was demonstrated in Chapter 3 that simply enumerating the different missile solutions allows for possible collisions between the missiles. Even if a missile collision does not occur, the missiles might approach too close to each other causing the missiles to respond in avoidance maneuvers in order to both prevent the possible collision and/or the aerodynamic effects from the air-stream of another missile. Since these effects must be prevented another methodology must be employed in solving the trajectory solution. A logical thought process would be to create a hierarchy amongst the missiles. The primary missile would be free in its trajectory solution from all the other missiles. Each sequentially ranked missile would solve its trajectory with the added constraint of ensuring that it's trajectory does not impede or collide with the previous missile trajectories.

This chapter focuses on solving a simplified case of the hierarchical approach between a lead missile (highest ranking) and a follow-on missile in a 2D cross-range and down-range for a minimum time trajectory solution. Using a hierarchical approach allows an additional constraint is placed upon the follow-on missile to keep a separation distance greater than some value R.

4.1 Primary Missile

The primary missile in the current scenario utilizes the same dynamics, constraints and starting conditions as missile 1 from Chapter 3, with the same target selection points of target A (2,1) and target B (2,0). The missile is free to progress in its trajectory to the chosen target with no regard on how its trajectory impinges on the secondary follow-on missile. Since the collision problem only arose in case 2 when missile 1 went to target B and missile 2 went to target A and did not have any possible collision issue when the missiles went to the targets with the longer time of arrival this chapter will only focus on resolving the collision issue for the case of missile 1 to target B and missile 2 to target A. This is reasonable because a primary and secondary missile problem setup will produce the same results since the primary and secondary setup is only to ensure that the secondary missile will prevent

a possible collision scenario. If no possible collision scenario exists, as in case 1, then no changes will occur in the optimal trajectories of the missiles. From this, all analysis for verification of the optimality of the primary missile is referred back to missile 1 in case 2 of Chapter 3.

4.2 Secondary Missile

Missile 2, the secondary/follow-on missile, has the added path constraint ($\mathcal{H}$) that ensures that the collision observed in Chapter 3 case 2 does not occur. The secondary missile is solved after the lead missile. The solution trajectory of the lead missile is inserted into the calculus of the secondary missile in order to maintain the minimum separation distance of R. The path constraint for modeling this separation distance is through a Euclidean distance function where the subscripts 1 and 2 refer to the lead and follow on missile respectively.

$$h(x, y) = (x_2 - x_1)^2 + (y_2 - y_1)^2 \tag{4.1}$$

where

$$\mathbf{h}^L = R^2. \tag{4.2}$$

The secondary missile problem can be written for a follow-on case as,

$$\mathbf{x}^T := [x, y, V, \theta] \in \mathbb{R}^4, \quad \mathbf{u} := \omega \in \mathbb{R} : |\omega| \leq \omega_{max}$$

$$\begin{cases} \text{Minimize} & J[\mathbf{x}(\cdot), \mathbf{u}(\cdot), t_f] = & t_f \\ \text{Subject to} & \dot{x} = & Vcos\theta \\ & \dot{y} = & Vsin\theta \\ & \dot{V} = & -(k_1 + k_2\omega^2)V^2 \\ & \dot{\theta} = & \omega \\ & V(t_0) = & V_0 \\ & t_0 = & 0 \\ & \mathbf{x}_0 = & (0, 0, c, d) \\ & e_1(\mathbf{x}_f) = & x_f - b = 0 \\ & e_2(\mathbf{x}_f) = & y_f - a = 0 \\ & \mathbf{h}^L \leq & h(x, y) \leq \infty \end{cases} \tag{4.3}$$

The Hamiltonian for the secondary missile is,

$$H_{Sec} = \lambda_{x2}V_2cos(\theta_2) + \lambda_{y2}V_2sin(\theta_2) - \lambda_{V2}(k_1 + k_2\omega_2^2)V_2^2 \tag{4.4}$$

which is the same as what was seen for missile 2 in Chapter 3. The difference occurs in the Lagrangian of the Hamiltonian for the secondary missile. Since the secondary missile has an additional constraint imposed upon it from the path constraint the Lagrangian of the Hamiltonian has an additional term imposed on it.

$$\begin{aligned} \bar{H}_{Sec} = \; & \lambda_{x2}V_2cos(\theta_2) + \lambda_{y2}V_2sin(\theta_2) - \lambda_{V2}(k_1 + k_2\omega_2^2)V_2^2 \\ & +\lambda_{\theta 2}\omega_2 + \mu_1\omega_2 + \mu_2((x_2 - x_1)^2 + (y_2 - y_1)^2) \end{aligned} \tag{4.5}$$

The KKT conditions for μ_1 and μ_2 are,

$$\mu_1 \quad \begin{cases} \leq 0, & \text{if} \quad \omega_2 = \omega_{\min}, \\ = 0, & \text{if} \quad \omega_{\min} < \omega_2 < \omega_{\max}, \\ \geq 0, & \text{if} \quad \omega_2 = \omega_{\max}, \end{cases} \tag{4.6}$$

and

$$\mu_2 \quad \begin{cases} \leq 0, & \text{if} \quad (x_2 - x_1)^2 + (y_2 - y_1)^2 = R^2, \\ = 0, & \text{if} \quad R^2 < (x_2 - x_1)^2 + (y_2 - y_1)^2. \end{cases} \tag{4.7}$$

Since there is no upper bound on the relative distance, i.e. the missiles have no limit on how far apart they can be separated, the value of μ_2 can never be positive.

Minimizing the Lagrangian of the Hamiltonian with respect to the control ω gives,

$$-2\lambda_{V2} k_1 \omega_2 V_2^2 + \lambda_{\theta 2} + \mu_1 = 0 = 0 \tag{4.8}$$

The adjoint equations are given in (4.9-4.12). The key difference between the secondary and primary missile is the effect that the constraint μ_2 has on the covectors λ_{x2} and λ_{y2}. Both of these covectors will be constant when the value of $\mu_2 = 0$ which will occur when the two missiles are separated by a distance greater than R!

$$-\dot{\lambda}_{x2} = \quad 2\mu_2(x_2 - x_1) \tag{4.9}$$

$$-\dot{\lambda}_{y2} = \quad 2\mu_2(y_2 - y_1) \tag{4.10}$$

$$-\dot{\lambda}_{V2} = \quad \lambda_{x2} cos\theta_2 + \lambda_{y2} sin\theta_2 - 2\lambda_{V2}(k_1 + k_2\omega_2^2)V_2 \tag{4.11}$$

$$-\dot{\lambda}_{\theta 2} = \quad -\lambda_{x2} V_2 sin\theta_2 + \lambda_{y2} V_2 cos\theta_2 \tag{4.12}$$

The Endpoint Lagrangian for the secondary missile differs from the primary only by the constant values in the respective endpoint constraint functions, $e_1(\mathbf{x}_f)$ and $e_2(\mathbf{x}_f)$.

$$\bar{E}_{Sec} \quad = t_f + \nu_1(x_{2f} - b) + \nu_2(y_{2f} - a) \tag{4.13}$$

This results in the Hamiltonian endpoint value being the same for the secondary missile as the primary missile.

$$\frac{dH}{dt} = 0 \tag{4.14}$$

$$\bar{H}(t_f) = -1 \tag{4.15}$$

The terminal transversality of the Endpoint Lagrangian results in the final costate values having the same form as the primary missile as is seen in Equations (4.16)-(4.19).

$$\lambda_{x2}(t_f) = \nu_1 \tag{4.16}$$

$$\lambda_{y2}(t_f) = \nu_2 \tag{4.17}$$

$$\lambda_{V2}(t_f) = 0 \tag{4.18}$$

$$\lambda_{\theta 2}(t_f) = 0 \tag{4.19}$$

Listed out, the boundary conditions for the secondary missile are,

$$\begin{aligned} &x_2(0) = 0; \quad y_2(0) = 0; \quad v_2(0) = c; \quad \theta_2(0) = d; \\ &x_2(t_f) = b; \quad y_2(t_f) = a; \quad \lambda_{v2}(t_f) = 0; \quad \lambda_{\theta 2}(t_f) = 0. \end{aligned} \tag{4.20}$$

4.2.1 Solution with Separation Distance R=0.025

Solutions for the two missiles were generated using DIDO and a separation distance of R = 0.025 was used. The missiles were set up the for case 2, with missile 1 going to Target B and missile 2 going to Target A. The solution for missile 1 remained the same as in Chapter 3. This solution was saved and used to generate missile 2's solution (Figure 4.1). This provides the information needed for the path constraint.

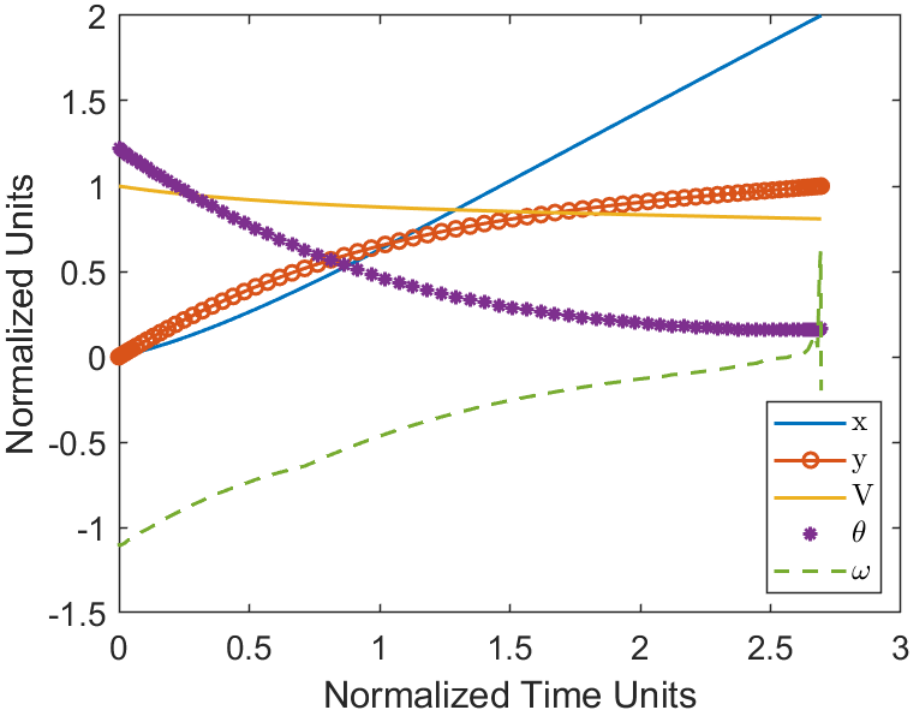

Figure 4.1. Secondary Missile States and Control

The secondary missile meets the costate requirements of Equations (4.9) and (4.10) in Figure 4.2a as well as the terminal transversality equations (4.18) and (4.19). The values for $\lambda_{V2}(t_f) = -7.86 \times 10^{-4}$ and $\lambda_{\theta 2}(t_f) = -1.22 \times 10^{-4}$. The Hamiltonian shows constancy within 10^{-2} of -1 as seen in Figure 4.2b.

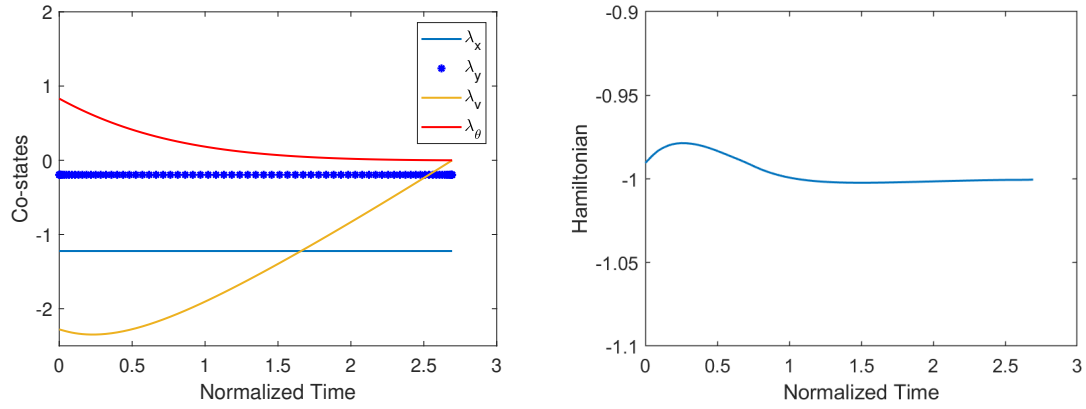

(a) (b)

Figure 4.2. Secondary Missile (a) Costates (b) Hamiltonian.

The values of the covectors μ_1 and μ_2 (Figures 4.3a and 4.3b) satisfy the respective complementarity conditions as seen in Equations (4.6) and (4.7). Specifically μ_2 is never positive.

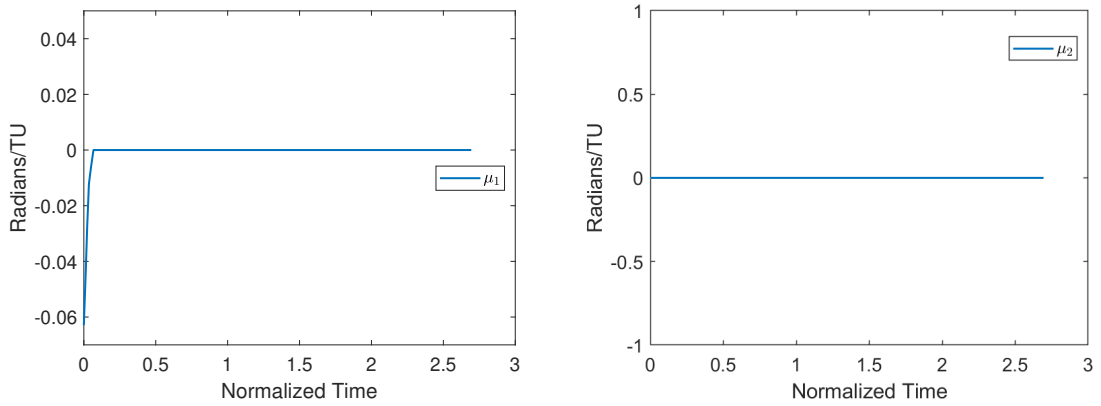

(a) (b)

Figure 4.3. Secondary Covectors (a) Plot of μ_1. (b)Plot of μ_2.

The final validation of the secondary missile solution was ensuring the that path constraint was satisfied, Equation (4.1). Namely that the separation distance between the missiles does not get closer than $R = 0.025$. Figure 4.4a shows that the secondary missile gets to a separation distance of R at scaled time 0.664. The secondary missile holds this distance

until scaled time 0.713 and then the missiles deviate. The control plot, Figure 4.4b for the secondary missile shows a sharp change at the scaled time 0.713 when the missiles' paths deviate. This 'kink' demonstrates that the control was effected by the path constraint to prevent the missile collision. The control for the secondary missile does show large jumps in value during the final moments in Figure 4.4b. The reasoning for this is that the affect of the control input at the final moments have very little effect on the missile's time. Also since the final control input is close to zero, control jumps between (+) and (−) values do not affect the time history within the tolerance values if the average is on the order of 0.

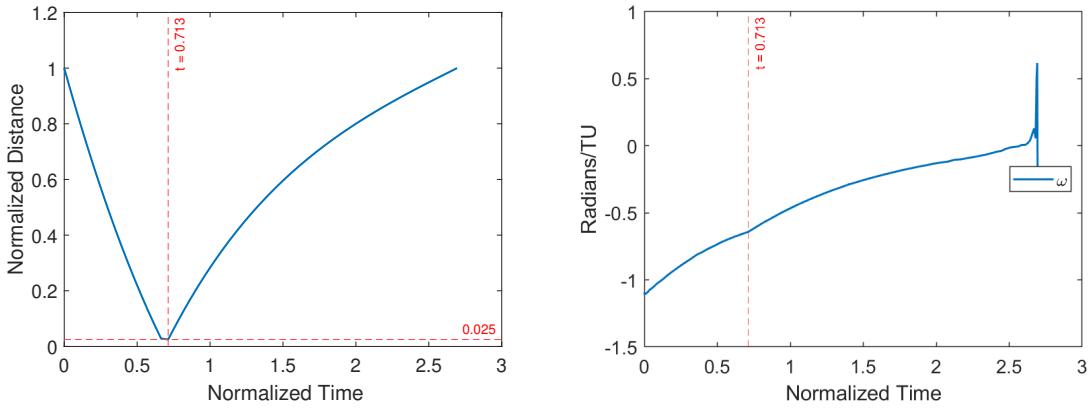

(a) (b)

Figure 4.4. (a) Separation Distance Between the Primary and Secondary Missiles (b) Secondary Control Vector at Closest Missile Approach

From the analysis the secondary missile solution provided by DIDO meets the conditions of optimality according to Pontryagin's Principle. The path of both missiles can be seen in Figure 4.5a. The paths of both missiles cross, but the path constraint ensured that the secondary missile crosses the primary missile's path after the primary missile has already passed, with the missiles coming to the minimum separation distance at $t = 0.713$ seen in Figure 4.5b.

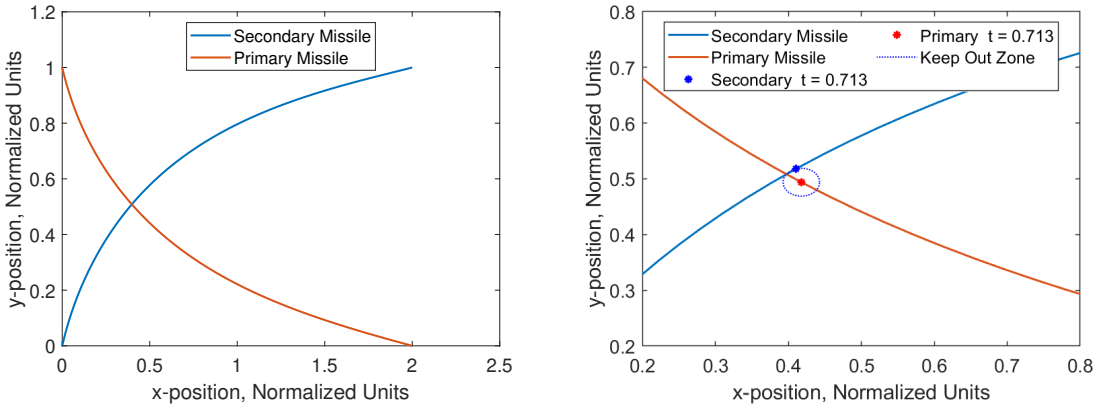

Figure 4.5. Position Plots of Primary and Secondary Missiles (a) Both Missiles Trajectories (b) Zoomed in with Separation Bubble During Closest Approach

4.2.2 Larger Values for Standoff Distance

The behaviors of the control and the covariable μ_2 in Figures 4.3b and 4.4b suggest that the trajectory shift required for the secondary missile to avoid collision is almost negligible for the current scaling. To look more deeply at the trajectory effects of a follow-on missile at different standoff distances of R were analyzed. It was noted that the time of flight for the secondary missile increased as the standoff distance was increased (Table 4.1).

It was also important to note that as the minimum separation distance increased the control history changed substantially in order for the secondary missile to avoid entering the no-fly space around the primary missile, Figure 4.6. Since the trajectories of the primary and secondary missiles spent more than just a moment at the separation distance, R, in these cases the path constraint covariable μ_2 was activated and a large negative jump is seen at the time of closest approach.

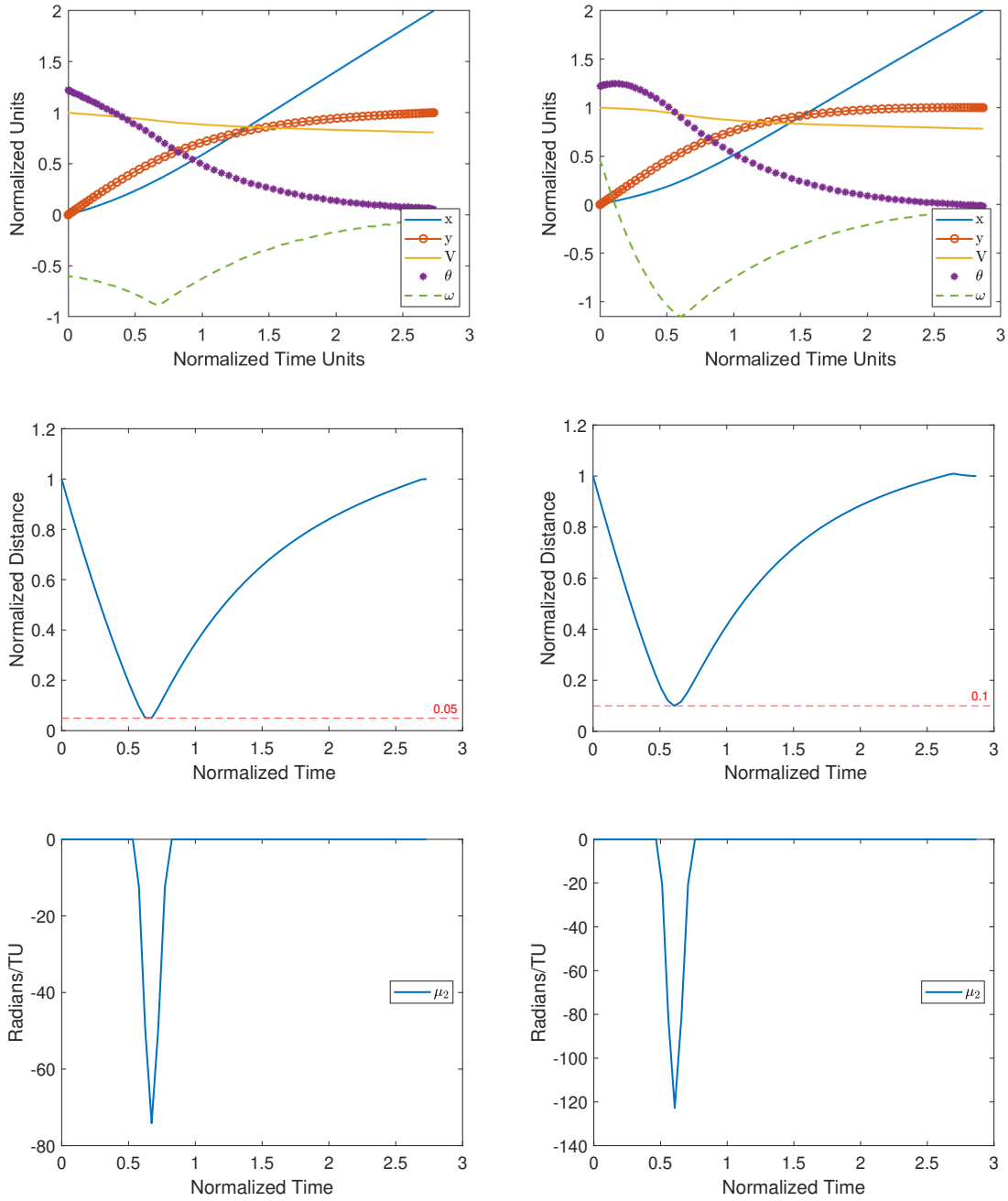

Figure 4.6. States and Control Histories, Separation Distance, and Path Constraint Covariable μ_2 for Different Stand Off Distances. Left: R = 0.05. Right: R = 0.1

Table 4.1. Secondary Missile's t_f

R	t_f
0.025	2.6942
0.050	2.7312
0.075	2.7948
0.100	2.8674

4.3 Delayed Start of the Follow-on Missile

The time of flight of the secondary missile in the final approach zone increases as the minimum required separation distance increases. This increased time in this zone could have negative consequences for the aggressor since it increases the probability that defender could intercept and defeat the incoming secondary missile. A possible solution to the longer time of flight problem is to allow the secondary missile to enter the final flight corridor at some variable time later than the primary missile. This additional time would allow the secondary missile to both not bleed off as much velocity to avoid the primary missile, but also allow it to not require as much control input deviation from the absence of the primary missile and allow it to travel less distance to get to its target.

Looking at the most extreme case of $R = 0.1$ for the minimum separation distance between the primary and secondary missile, the secondary missile's initial conditions were loosened in y and in t_0. The starting y position was allowed to start anywhere between $y = 0$ and $y = \delta = 0.2$. Since the starting position of the secondary missile is loosened, the time it enters the final flight corridor must be adjusted relative to the lead missile's starting t_0. This can be simulated through the relation of

$$y_{2o} = V \times \Delta t.$$

Since $V_0 = 1$ the time delay between the two missiles' start time is just the numerical value of the starting y_{2o}.

4.3.1 Application of Pontryagin's Principle to the Delayed Start Scenario

The initial y position and initial time of the secondary missile not being fixed meant that event functions needed to be added to the OCP for the secondary missile.

$$e_3(y_{2o}) = y_{2o} \tag{4.21}$$
$$e_4(t_0) = t_0 - y_{2o} \tag{4.22}$$

The constraints on the event functions as seen in Equation (4.23) are from the allowed 'wiggle room' in the missile's starting time and position.

$$\begin{aligned} 0 \leq \quad & e_3(y_{2o}) \leq \quad \delta \\ 0 \leq \quad & e_4(t_0) < \quad \infty \end{aligned} \tag{4.23}$$

The new problem retained the same Hamiltonian and Lagrangian of the Hamiltonian. Therefore, the application of Pontryagin's Principle retained the same Equations (4.4)-(4.12) as the previous iteration of the secondary missile problem. The new Endpoint Lagrangian can be seen in Equation (4.25) from the additional event functions.

$$\bar{E}_{Sec} = t_f + \nu_1(x_{2f} - b) + \nu_2(y_{2f} - a) + \nu_3(y_{2o}) + \nu_4(t_0 - y_{2o}) \tag{4.24}$$
$$+\nu_5(x_{2o}) + \nu_6(V_{2o} - c) + \nu_7(\theta_{2o} - d) \tag{4.25}$$

Since the added event functions for initial t_0 and y_{2o} are constrained with $\mathbf{e}^L \neq \mathbf{e}^U$ the values of ν_3 and ν_4 were constrained according to the KKT conditions. The KKT conditions for the ν values are,

$$\nu_3 \quad \begin{cases} \leq 0, & \text{if} \quad y_{2o} = 0, \\ = 0, & \text{if} \quad 0 < y_{2o} < \delta, \\ \geq 0, & \text{if} \quad y_{2o} = \delta, \end{cases} \tag{4.26}$$

and

$$\nu_4 \quad \begin{cases} \leq 0, & \text{if} \quad t_0 - y_{2o} = 0, \\ = 0, & \text{if} \quad t_0 - y_{2o} > 0. \end{cases} \tag{4.27}$$

The other initial ν values are unrestricted since the corresponding states are restricted with $\mathbf{e}^L = \mathbf{e}^U$.

The final endpoints of the Endpoint Lagrangian remained the same, resulting in the final Hamiltonian value and the terminal transversality of the Endpoint Lagrangian, (4.15)-(4.19), also remaining the same. The addition of initial endpoint constraints required that the initial Hamiltonian value be analyzed according to Equation (4.28). The result was that the Hamiltonian started at some unknown value ν_4, Equation (4.29).

$$\bar{H}(t_o) = \frac{\partial \bar{E}}{\partial t_o} \tag{4.28}$$

$$\bar{H}(t_o) = \nu_4 \tag{4.29}$$

The Initial Transversality of the Endpoint Lagrangian was analyzed according to Equation (4.30).

$$\boldsymbol{\lambda}(t_o) = \frac{\partial \bar{E}}{\partial \mathbf{x_o}} \tag{4.30}$$

The resulting Initial Transversality for $\boldsymbol{\lambda}(t_0)$, Equations (4.31) - (4.34), gave no information for the corresponding x, V, θ initial costate values. While the values of ν_3 and ν_4 are not explicitly known, they are constrained with their respective KKT conditions giving some information on the value of $\lambda_{y2}(t_0)$.

$$\lambda_{x2}(t_0) = \nu_5 \tag{4.31}$$

$$\lambda_{y2}(t_0) = \nu_3 - \nu_4 \tag{4.32}$$

$$\lambda_{V2}(t_0) = \nu_6 \tag{4.33}$$

$$\lambda_{\theta 2}(t_0) = \nu_7 \tag{4.34}$$

4.3.2 DIDO Results for a Delayed Start

The DIDO solution was solved with a start time of $t_0 = 0.1084$ and a starting y-position of $y = 0.0779$, with a t_{2f} of 2.8068. The DIDO solution met the required conditions of optimality as seen in Figure 4.7. The closest approach of the two missiles was from $t = 0.6343$ until $t = 0.680$. Figures 4.7c-4.7f show this by having sharp discontinuities in their time histories at the approach and separation when the covector μ_2 activates.

The change in the value of the Hamiltonian seen in Figure 4.7b might appear to violate the Hamiltonian evolution in Equation (4.14) that requires the Hamiltonian to have derivative of 0. However, the jump in the Hamiltonian value is allowable since it is due to the impulse generated by the activation of μ_2 that occurs when the secondary missile reaches the standoff distance. The initial and final Hamiltonian values are met with the Hamiltonian remaining constant except for the jump discontinuity.

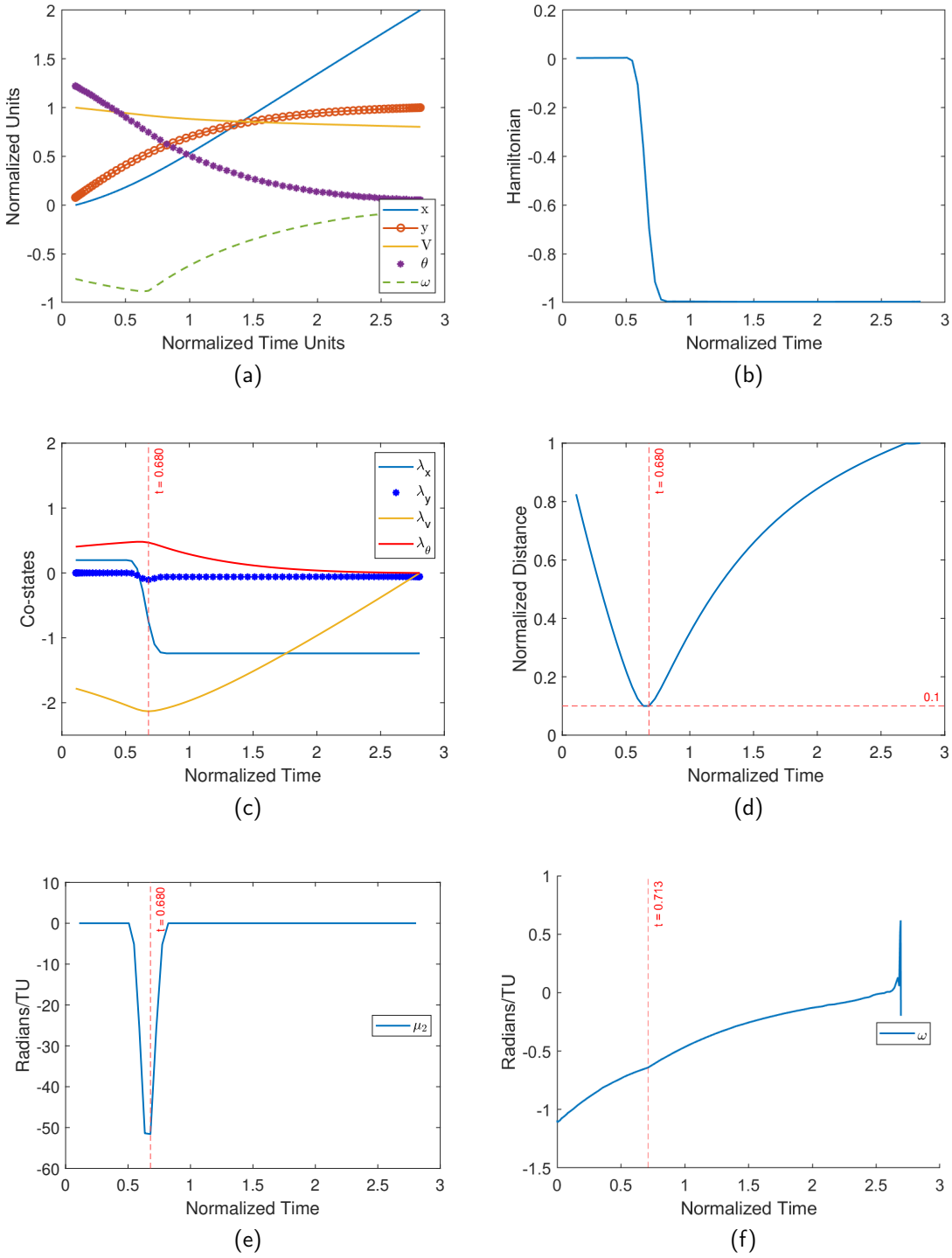

Figure 4.7. Secondary Missile with R =0.1 Minimum Separation Distance with Delayed Start. (a) States and Control (b) Hamiltonian (c) Costates (d) Missile Separation (e) Covector μ_2 (f) Control

The windowed start option for the secondary missile with the primary missile are shown in Figure 4.8 starting at $t = 0.1084$. The primary missile has already traveled some distance before the start time of the secondary missile is reached as is shown by the primary missile not starting at [0, 1]. The interesting effect of this delayed start is that the secondary missile both in arrives sooner and has a shorter time of flight in the final flight corridor as time shown in Table 4.2.

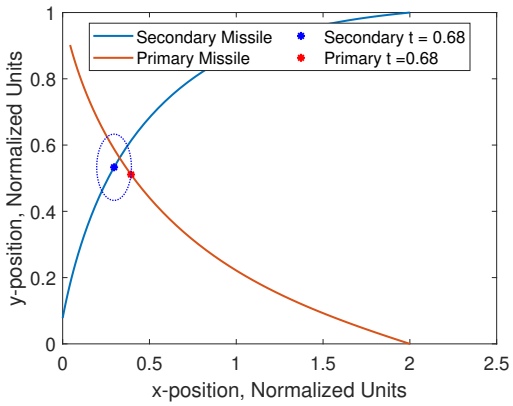

Figure 4.8. Primary and Secondary Missile with Delayed Start from $t = 0.1084$ to Target Impact

Table 4.2. Arrival Time and Flight Time of Fixed and Delayed Start of the Secondary Missile

	t_f	Flight Time
$t_0 = 0$	2.8674	2.8674
$t_0 = 0.1084$	2.8068	2.6982
Δ	0.0606	0.1692

4.4 Chapter Summary

From this it can be seen that the simultaneous time of arrival for the primary and the secondary missile cannot be ensured with the method of lead and follow-on trajectory optimization. Instead of the problem scenario being a LSAP it is now a *linear bottle neck*

assignment problem (LBAP). A LBAP differs from the LSAP in that while the LSAP seeks to optimize the sum of costs of all of the agents, a LBAP seeks only to optimize the largest cost of a set of agents, which in this case is seeking to minimize the t_f of the last missile to reach its target.

Utilizing the lead and follow-on missile methodology still requires an enumeration over all possible missile-target combinations. In addition the enumeration calls increase with the use of a lead and follow-on missile methodology. In the case of a non-symmetric problem set, either from the flight corridor and target location geometries, or in non-symmetric missile dynamics the selection of the lead missile will determine the overall missile strike time. This will have to be optimized by now enumerating over each case with every missile being rotated through being the lead. This greatly increases the number of enumeration, with cases of an large $n \times n$ system quickly becoming extremely computationally expensive. In the next chapter an alternative approach is explored through the modeling of the individual missile dynamics in a system of systems.

THIS PAGE INTENTIONALLY LEFT BLANK

CHAPTER 5:
System of Systems

This chapter focuses on a methodology for solving the multiple missile trajectories concurrently while still maintaining the simultaneous time of arrival that the hierarchical approach of Chapter 4 failed to maintain. This method is similar to the previous techniques demonstrated, but expands the problem system from one missile, to a problem system in which each of the missiles are sub-systems. The advantage of this methodology is the path constraint $\mathcal{H}$ is able to be implemented directly with no extra interpolation, or calls outside of the inner loop solution, i.e. the missiles are solved in parallel rather than sequentially.

5.1 System of Systems Problem

A way to model both missiles simultaneously, while also accounting for the minimum required separation distance of between the pair is to solve the problem as a system made up of each individual missile system, i.e. a system-of-systems. This is effectively combining the OCP's dynamics and constraints of each missile into a single OCP that contains both missiles.

$$\mathbf{x}^T := [x, y, V, \theta] \in \mathbb{R}^4, \quad \mathbf{u} := \omega \in \mathbb{R} : |\omega| \leq \omega_{max}$$

$$OCP\ to\ Target\ P \begin{cases} \text{Minimize} & J[\mathbf{x}(\cdot), \mathbf{u}(\cdot), t_f] = & t_f \\ \text{Subject to} & f_{missile1}(\mathbf{x}_1, \mathbf{u}_1, t) = & \mathcal{D}_1 \\ & f_{missile2}(\mathbf{x}_2, \mathbf{u}_2, t) = & \mathcal{D}_2 \\ & t_0 = & 0 \\ & \mathbf{x}_1(t_0) = & HGV_1(t_0) \\ & \mathbf{x}_2(t_0) = & HGV_2(t_0) \\ & \mathbf{e}_1(x_{1f}, y_{1f}) = & HGV_1(t_f) - P_i = 0 \\ & \mathbf{e}_2(x_{2f}, y_{2f}) = & HGV_2(t_f) - P_j = 0 \\ & \mathbf{h}^L \leq & h(x_1, y_1, x_2, y_2) \leq \infty \end{cases} \tag{5.1}$$

where $i \neq j$, each target must be hit so both missiles cannot go to the same target endpoint.

$$
\begin{array}{c}
HGV \\
\mathcal{H}_i
\end{array}
\left\{
\begin{array}{lll}
\dot{x}_i = & V_i cos\theta_i \\
\dot{y}_i = & V_i sin\theta_i \\
\dot{V}_i = & -(k_1 + k_2\omega_i^2)V_i^2 \\
\dot{\theta}_i = & \omega_i
\end{array}
\right.
\qquad
\begin{array}{c}
Boundary \\
Conditions
\end{array}
\left\{
\begin{array}{lll}
x_0, y_0 = & HGV_1^0 \vee HGV_2^0 \\
V_0, \theta_0 = & (c, \pm d) \\
x_f, y_f = & A \vee B \\
V_f, \theta_f = & \text{free}
\end{array}
\right.
$$

The construction of the Hamiltonian for the system-of-systems is the summation of the Hamiltonians of the individual missiles.

$$H_{System} = \lambda_1^T f_{missile1}(\mathbf{x}_1, \mathbf{u}_1, t) + \lambda_2^T f_{missile2}(\mathbf{x}_2, \mathbf{u}_2, t) \tag{5.2}$$

$$
\begin{aligned}
H_{System} = \quad & \lambda_{x_1} V_1 cos(\theta_1) + \lambda_{y_1} V_1 sin(\theta_1) - \lambda_{V_1}(k_1 + k_2\omega_1^2)V_1^2 + \lambda_{\theta_1}\omega_1 \\
& \lambda_{x_2} V_2 cos(\theta_2) + \lambda_{y_2} V_2 sin(\theta_2) - \lambda_{V_2}(k_1 + k_2\omega_2^2)V_2^2 + \lambda_{\theta_2}\omega_2
\end{aligned} \tag{5.3}
$$

Likewise the Lagrangian of the Hamiltonian is simply the sum of the individual Lagrangians with the addition of the covariable term for the minimum separation distance μ_3.

$$
\begin{aligned}
\bar{H}_{system} = \quad & \lambda_{x_1} V_1 cos(\theta_1) + \lambda_{y_1} V_1 sin(\theta_1) - \lambda_{V_1}(k_1 + k_2\omega_1^2)V_1^2 + \lambda_{\theta_1}\omega_1 \\
& \lambda_{x_2} V_2 cos(\theta_2) + \lambda_{y_2} V_2 sin(\theta_2) - \lambda_{V_2}(k_1 + k_2\omega_2^2)V_2^2 + \lambda_{\theta_2}\omega_2 \\
& +\mu_1\omega_1 + \mu_2\omega_2 + \mu_3((x_1 - x_2)^2 + (y_1 - y_2)^2)
\end{aligned} \tag{5.4}
$$

The KKT conditions for the covariables, μ_i, are the same as seen in Chapters 3 and 4.

$$
\text{For } i = 1, 2 \quad \mu_i \quad
\begin{cases}
\leq 0, & \text{if} \quad \omega_i = \omega_{\min}, \\
= 0, & \text{if} \quad \omega_{\min} < \omega_i < \omega_{\max}, \\
\geq 0, & \text{if} \quad \omega_i = \omega_{\max}
\end{cases} \tag{5.5}
$$

$$\mu_3 \quad \begin{cases} \leq 0, & \text{if} \quad h(\mathbf{x}) = R^2, \\ = 0, & \text{if} \quad R^2 < h(\mathbf{x}). \end{cases} \tag{5.6}$$

The difference in the result for applying the HMC to the system-of-system's OCP is that it is a vector of equations. Each entry in the vector is the HMC solution for the individual missile.

$$\frac{\partial \bar{H}}{\partial \mathbf{u}} = \begin{bmatrix} -\lambda_{V_1} k_2 \omega_1 V_1^2 + \lambda_{\theta_1} + \mu_1 \\ -\lambda_{V_2} k_2 \omega_2 V_2^2 + \lambda_{\theta_2} + \mu_2 \end{bmatrix} = \begin{bmatrix} 0 \\ 0 \end{bmatrix} \tag{5.7}$$

Likewise, the adjoint equations become a system of adjoint systems.

$$-\dot{\boldsymbol{\lambda}}(\mathbf{x}, \mathbf{u}) = \begin{bmatrix} 2\mu_3 \\ 2\mu_3 \\ \lambda_{x_1} cos\theta_1 + \lambda_{y_1} sin\theta_1 - 2\lambda_{V_1}(k_1 + k_2\omega_1^2)V_1 \\ -\lambda_{x_1} sin\theta_1 + \lambda_{y_1} cos\theta_1 \\ -2\mu_3 \\ -2\mu_3 \\ \lambda_{x_2} cos\theta_2 + \lambda_{y_2} sin\theta_2 - 2\lambda_{V_2}(k_1 + k_2\omega_2^2)V_2 \\ -\lambda_{x_2} sin\theta_2 + \lambda_{y_2} cos\theta_2 \end{bmatrix} = \begin{bmatrix} -\dot{\lambda}_{x_1} \\ -\dot{\lambda}_{y_1} \\ -\dot{\lambda}_{V_1} \\ -\dot{\lambda}_{\theta_1} \\ -\dot{\lambda}_{x_2} \\ -\dot{\lambda}_{y_2} \\ -\dot{\lambda}_{V_2} \\ -\dot{\lambda}_{\theta_2} \end{bmatrix} \tag{5.8}$$

The Endpoint Lagrangian, Equation (5.9), and the terminal transversality of the Endpoint Lagrangian, Equation (5.10), for the system-of-systems simply adds the event conditions for each missile into the single Endpoint Lagrangian.

$$\bar{E}_{System} = t_f + \nu_1(x_{1f} - x_1^f) + \nu_2(y_{1f} - y_1^f) + \nu_3(x_{2f} - x_2^f) + \nu_4(y_{2f} - y_2^f) \tag{5.9}$$

$$\frac{\partial \bar{E}}{\partial \mathbf{x}_f} = \begin{bmatrix} \nu_1 \\ \nu_2 \\ 0 \\ 0 \\ \nu_3 \\ \nu_4 \\ 0 \\ 0 \end{bmatrix} = \begin{bmatrix} \lambda_{x_1}(t_f) \\ \lambda_{y_1}(t_f) \\ \lambda_{V_1}(t_f) \\ \lambda_{\theta_1}(t_f) \\ \lambda_{x_2}(t_f) \\ \lambda_{y_2}(t_f) \\ \lambda_{V_2}(t_f) \\ \lambda_{\theta_2}(t_f) \end{bmatrix} \tag{5.10}$$

5.2 Case 1

Solving the system-of-systems for case 1 with missile 1 paired to target A and missile 2 paired to target B produces the exact trajectory path as seen in the simple enumeration method with the same time of flight with $t_f = 2.898$. This is to be expected since no interaction between the missiles is required in terms of collision avoidance.

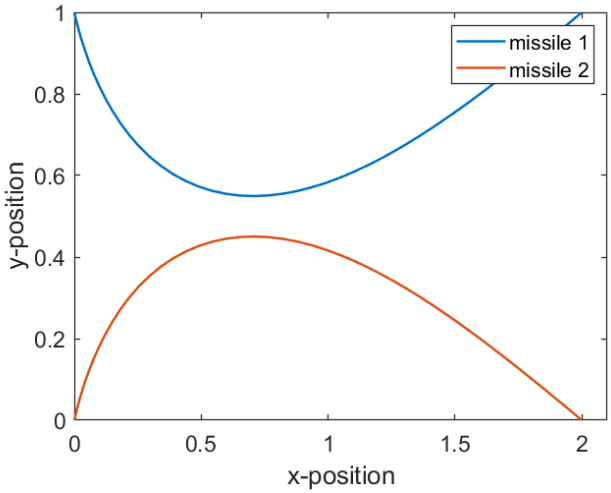

Figure 5.1. Missile Trajectories for Case 1 Using the System-of-systems Model.

Analyzing this trajectory solution demonstrated that optimality was met. Looking at Figures 5.2c and 5.2e, it can be seen that the costates match with theory for the adjoint equations, Equation (5.8), i.e. λ_x and λ_y for each missile were constant. The terminal transversality equation was met, Equation (5.10), since λ_V and λ_θ both have a terminal value of 0. Comparing Figure 5.2 with the KKT conditions for the limited control input, Equation (5.5), is consistent with theory.

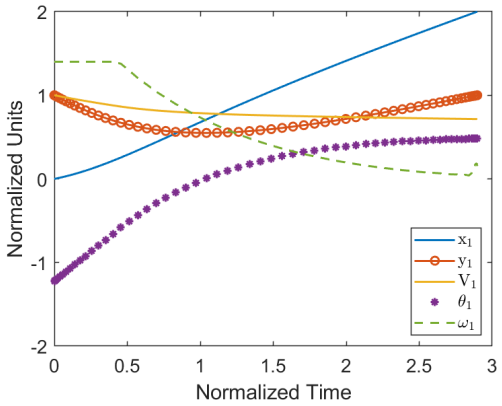

(a) States and Control

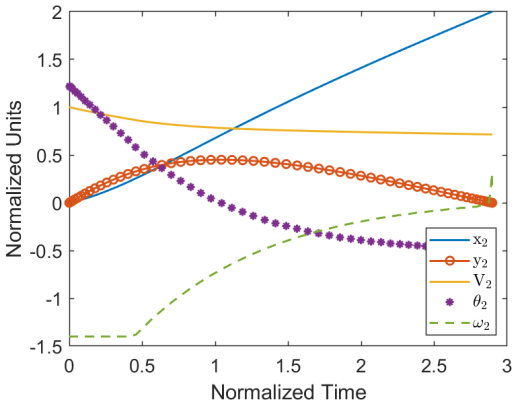

(b) States and Control

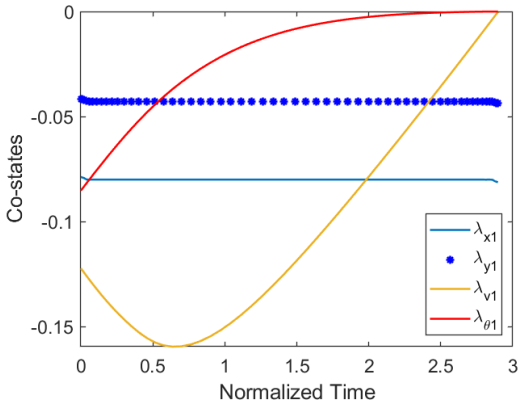

(c) Costates

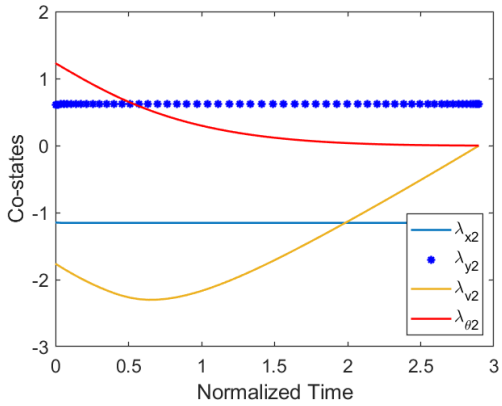

(d) Costates

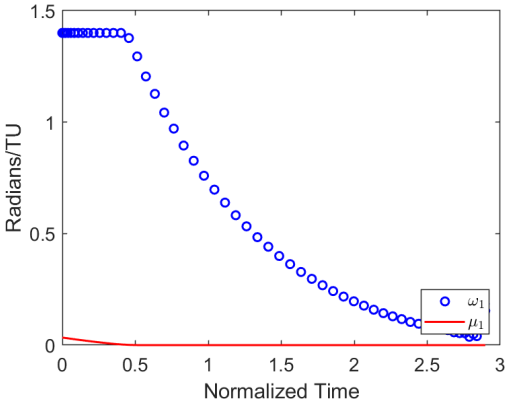

(e) Control and Covariable

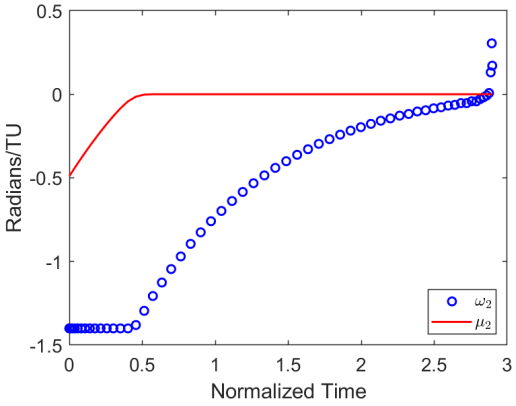

(f) Control and Covariable

Figure 5.2. Optimality Plots for Case 1 of System-of-systems. Left: Missile 1 Goes to Target A. Right: Missile 2 Goes to Target B.

The separation requirement for the missiles was obviously met, with the missiles not getting to a distance R of each other, therefore the respective covariable μ did not show any activation, Figure 5.3b. The Hamiltonian was also consistent with theory at a constant $H(t) = -1$, Figure 5.3a.

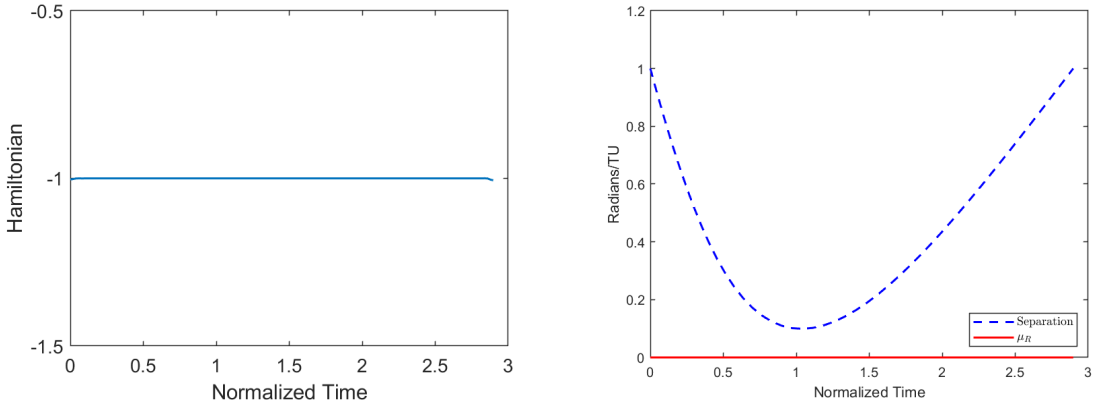

Figure 5.3. System-of-systems Case 1 (a) Hamiltonian (b) Separation and Corresponding Path Covector μ

5.3 Case 2

The Case 2 missile scenario was also successfully solved with $t_f = 2.693$. The trajectory solution crosses as seen in Figure 5.4a, but looking at the time of closest approach one sees that the missiles are at a separation distance of R at $t = 0.710$ (Figure 5.4b). The missiles never get closer than a distance R from each other (Figure 5.4c).

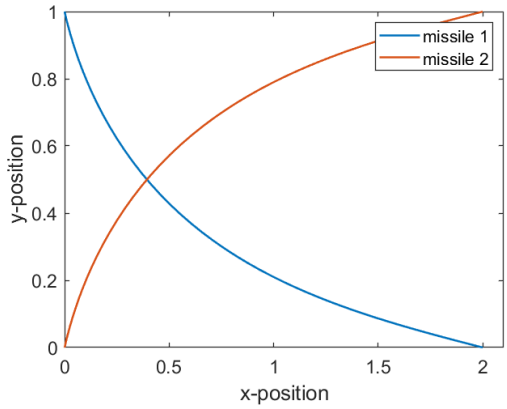

(a)

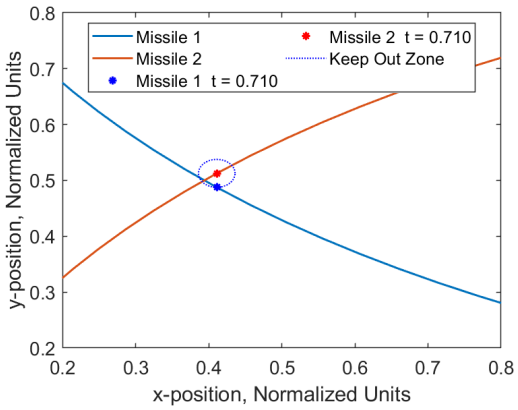

(b)

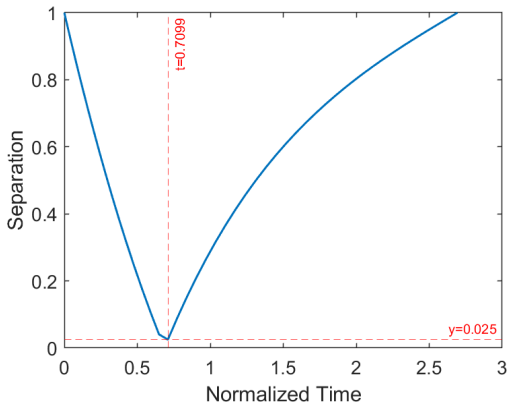

(c)

Figure 5.4. Missile Trajectories and Separation Distance for Case 2 Using the System-of-systems Model

Analysis of this trajectory solution shows that the conditions for optimality were met. Looking at Figures 5.5c and 5.5d it can be seen that the costates match with theory for the adjoint equations, Equation (5.8), since λ_x and λ_y for each missile were constant. It can also be observed that the terminal transversality condition, Equation (5.10), was met since λ_V and λ_θ both have a terminal value of 0. Comparing Figures 5.6a, 5.6b and 5.6d with the KKT conditions for the limited control input, Equation (5.5), shows that the covariables have values consistent with theory since μ_1 and μ_2 are never activated from reaching a control bound, while μ_R activates when the standoff limit is reached.

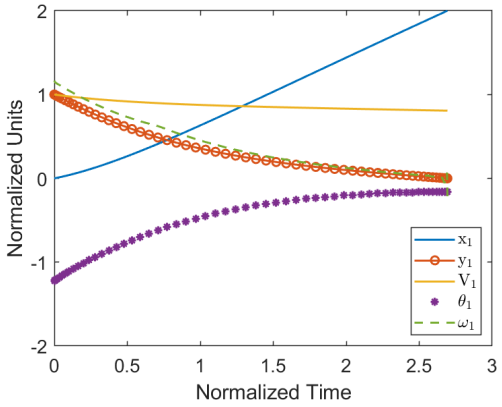

(a) States and Control Missile 1

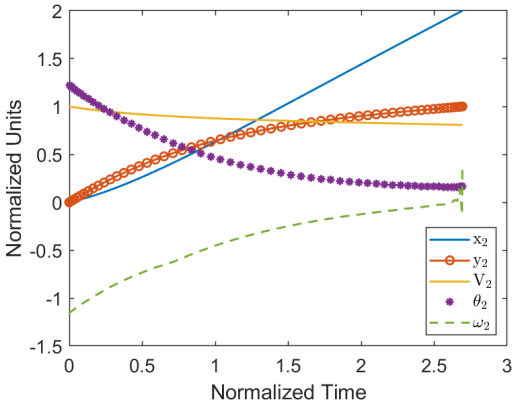

(b) States and Control Missile 2

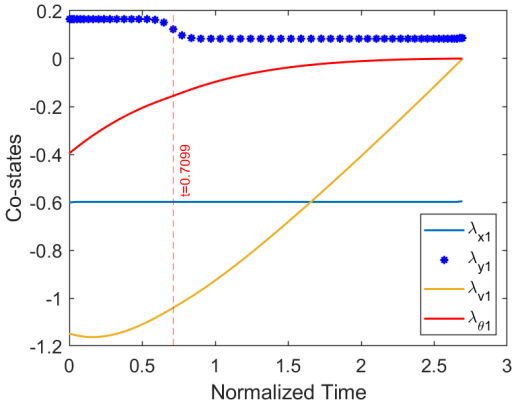

(c) Costates Missile 1

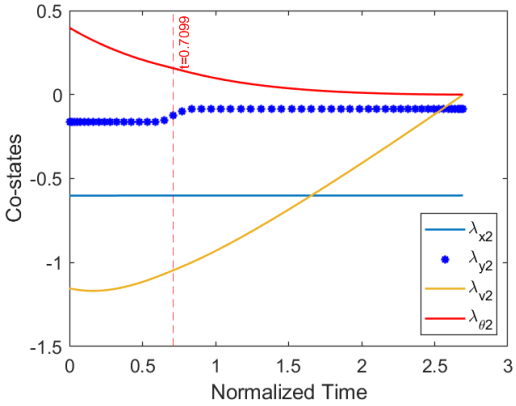

(d) Costates Missile 2

Figure 5.5. System-of-systems Case 2 States and Costates

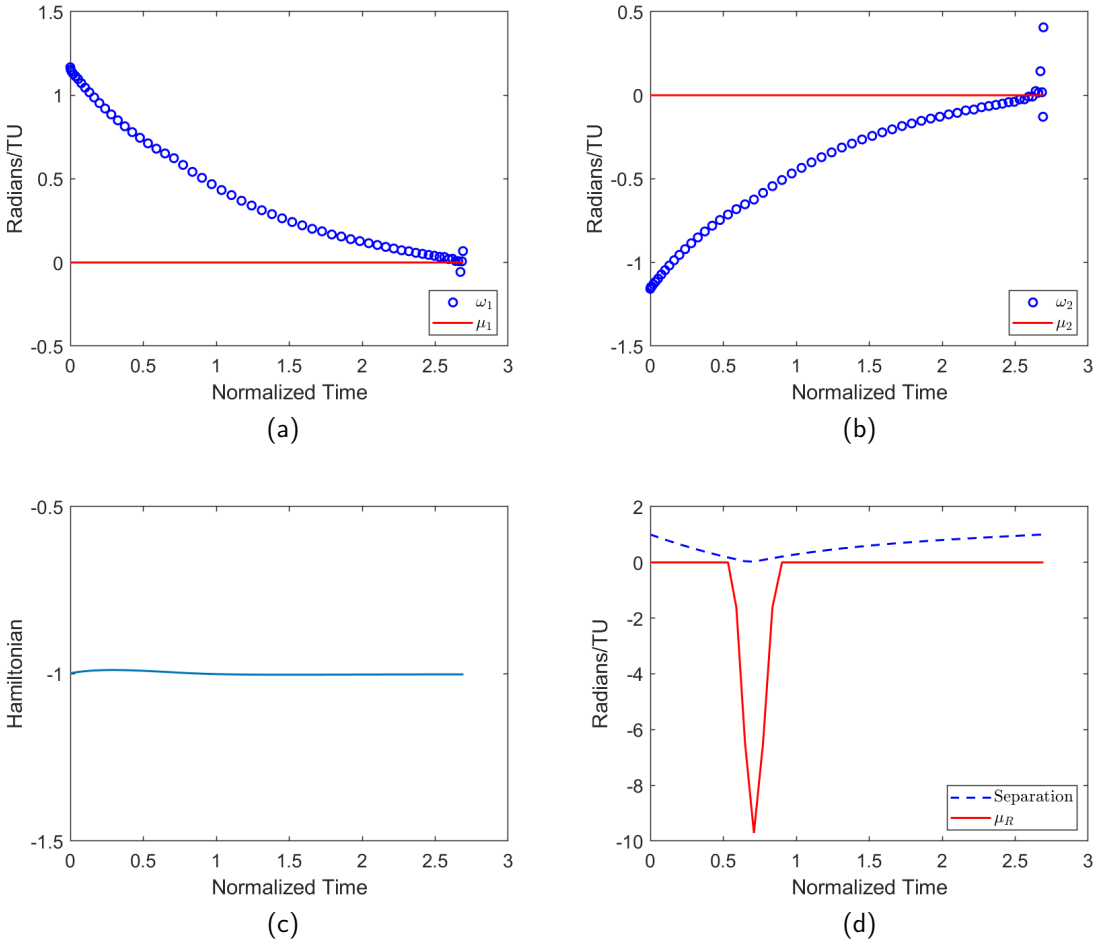

Figure 5.6. System-of-systems Case 2 (a) Control and Covariable μ_1 for Missile 1. (b) Control and Covariable μ_2 for Missile 2. (c) Hamiltonian (d) Separation and Corresponding Path Covector μ

5.4 Chapter Summary

A big advantage seen in the system-of-systems model over the lead and follow-on method of Chapter 4, is that both missiles are able to control their maneuvers to avoid collision. This equates to a faster time of arrival for the missiles than only having one missile perform collision avoidance, as well as allows for simultaneous time on target.

This methodology still requires an enumeration over all possible missile-target combinations. It does reduce the number of inner-loop calls that would be required since the enumerations have been reduced by turning the problem into a system, thereby cutting the calls in half compared to Chapter 3. This is a major reduction in the number of calls compared the lead and follow-on methodology in Chapter 4.

CHAPTER 6:
Target Selection Using a Designer Endpoint Function

Enumerating over the different missile to target combinations in the system-of-missiles problem setup reduces the overall number of inner loop calls in the solved trajectory costs down from n^2 to n. The actual target selection is still performed in an outer loop call, a so called *"racking and stacking"* of the diagonals in the conventional cost matrix. The disparate end points for each missile are still solved individually, with the other missile being solved in parallel.

This chapter continues the trajectory solution to the simple glide missile model by showing how the individual target endpoints of the missiles can be solved simultaneously. This is done by using a user selected Designer Function ($\mathcal{F}(\mathbf{x})$), for the endpoints to map the disparate points onto a continuous curve, thereby turning the exclusive *XOR* statement into a conjunctively true *AND* statement. The conversion of the binary nature of the XOR statement into a continuous mapping allows the OCP to meet the stringent requirements of optimization through a continuous algebra without an enumeration methodology.

6.1 Developing an Endpoint Designer Function

Since the OCP can only solve conjunctively true statements one must turn the *XOR* statement of the distinct target endpoints and turn them into an *AND* statement, or series of *AND* statements in order to solve the problem without utilizing one of the previous chapters enumeration methods. This can be done with what we call a Designer Function. This is a function, or set of functions, that the engineer/operator develops based around the dynamics and constraints of the system, so that the disparate nature of target endpoints can be mapped to a continuous curve in order to meet the differentiable requirement of solving the problem. A properly constructed function will allow the solver to map the correct time optimal control history for an optimal solution according to the problem constraints. When the Designer Endpoint Function is taken with the other functional constraints that are imposed upon the system, namely the event functions $\mathcal{E}$ and the path constraints $\mathcal{H}$, the *XOR* statement is converted into a *AND* statement, and therefore becomes conjunctively true [18].

Investigations into what needs to be ensured in a proper $\mathcal{F}(\mathbf{x})$ have demonstrated that one can improperly setup the problem if the Designer Function is not constructed appropriately for the given problem framework [27]. Specifically, the partial of $\mathcal{F}(\mathbf{x})$ with respect to an end-state and the partial of the remaining $\mathcal{E}(\mathbf{x})$ both cannot both be a zero vector, Equations 6.1 and 6.2.

$$\frac{\partial \mathcal{F}(x)}{\partial x_f} \neq 0 \tag{6.1}$$

and

$$\frac{\partial \boldsymbol{e}(x)}{\partial x_f} \neq 0. \tag{6.2}$$

Issues arise if the Hamiltonian solution requires that the corresponding final costate value

$$\lambda_x(t_f) \neq 0$$

and Equations 6.1 and 6.2 are not met. Mathematically the event multiplier ν_x must become infinity since

$$\lambda_x(t_f) = \lim_{x \to x_f} \nu_x(x) \cdot \lim_{x \to x_f} \frac{\partial \mathcal{F}(x)}{\partial x} \neq 0$$

while

$$\frac{\partial \mathcal{F}(x)}{\partial x_f} = 0.$$

Therefore, when constructing the $\mathcal{F}(\mathbf{x})$ the problem architect must ensure that one of Equations 6.1 and 6.2 are met.

Looking at the example problem, the missiles are supposed to go to target A or target B. The missiles not allowed to go to the same location, or come within a set distance R of each other. An initial attempt at solving this problem without explicitly stating which missiles goes to which target, is to take the OCP from Chapter 5 and replace the explicit endpoint constraints of the event functions $\mathcal{E}$ with a problem specific $\mathcal{F}(\mathbf{x})$. This $\mathcal{F}(\mathbf{x})$ maps the disparate endpoints for targets A and B onto a set of continuous curves/functions that turns the *XOR* statement into a conjunctively true system of *AND* statements contained within the OCP.

6.2 Results Using Designer Function 1

A preliminary $\mathcal{F}(\mathbf{x})$ is to construct a line segment that contains both target endpoints on the line. For this case, each target endpoint coincides with the endpoints of the line segment. In addition to this event function is to then construct a circle centered between the target points with the condition that the missile must not end inside of the circle, i.e., an ending exclusion zone. When taken together, the circle and the line would map two distinct continuous sets for where the missiles are allowed to end (Figure 6.1a). The intersection of these two regions would limit the missiles to a smaller set for where they are allowed to end, namely the intersection of the region outside of the circle and the line segment δ are where the missiles can end their maneuvers, seen in Figure 6.1b.

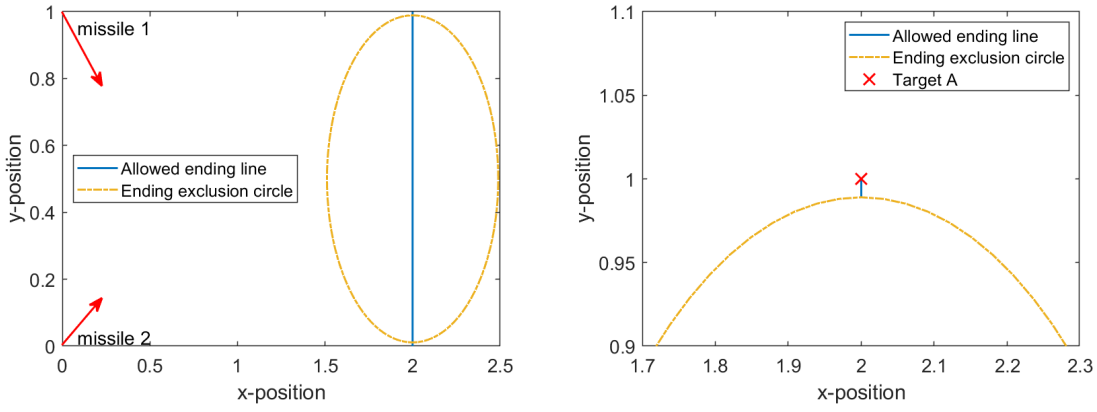

Figure 6.1. (a) Missile Endpoint Functions. (b) Zoomed in Showing the Allowed δ.

This system of event functions that must be satisfied creates the $\mathcal{F}(\mathbf{x})$ for each missiles target selection. However, the tolerances of DIDO does not allow the intersection of the line segment and the endpoint exclusion circle to intersect only at the endpoints of the line segment. This means that the radius of the exclusion circle is $R_{exclude} = \frac{\text{Line segment}}{2} - \delta$, where δ is the minimum separation that the solver requires between the exclusion circle and the target endpoint seen in Figure 6.1b. These conditions result in the following Designer

Endpoint Function,

$$\mathcal{F}_1(\mathbf{x}_1) = \begin{bmatrix} x_{1f} - b \\ y_{1f} \\ (x_{1f} - b)^2 + (y_{1f} - 0.5)^2 - (0.5 - \delta)^2 \end{bmatrix} \tag{6.3}$$

and

$$\mathcal{F}_1(\mathbf{x}_2) = \begin{bmatrix} x_{2f} - b \\ y_{2f} \\ (x_{2f} - b)^2 + (y_{2f} - 0.5)^2 - (0.5 - \delta)^2 \end{bmatrix} \tag{6.4}$$

where

$$e^L \leq \mathcal{F}_1(\mathbf{x}) \leq e^U \tag{6.5}$$

$$\begin{bmatrix} 0 \\ 0 \\ 0 \\ 0 \\ 0 \\ 0 \end{bmatrix} \leq \mathcal{F}_1(\mathbf{x}) \leq \begin{bmatrix} 0 \\ 1 \\ \infty \\ 0 \\ 1 \\ \infty \end{bmatrix}. \tag{6.6}$$

This small error means that the missiles are not being told by the problem formulation to actually hit the targets, rather to hit a region that extends past the target by a distance δ. As long as this δ error is smaller than the minimum separation distance, R, the missiles are forced to go to separate target regions. Initial attempts using this method showed simultaneous time of arrival with minimum time of flight being met for this formulation of $\mathcal{F}(\mathbf{x})$, however the missiles in this problem set would hit right at the edge of the exclusion circle on the allowed line segment a distance of δ away from the target. The missiles chose the correct targets when compared to the system-of-systems baseline from Chapter 5 and so this small error in targeting might be allowable in certain mission considerations as long as the scaling of the problem solution produces a distance δ that is less than the error margins on the real missile controller. It must be stated that no proof of optimality was investigated

in this case, since focus was put into removing the small error and getting the missiles to actually hit the target.

An attempt to fix the δ error was by adding a Mayer cost to the cost functional J. This transformed the cost functional to

$$J = \beta[(y_{1\,f} - y_{\text{Target A}})^2(y_{1\,f} - y_{\text{Target B}})^2 + (y_{2\,f} - y_{\text{Target A}})^2(y_{2\,f} - y_{\text{Target B}})^2] + t_f$$

where the subscripts 1 and 2 correspond to missiles 1 and 2 respectively. The thought process behind this additional term to the cost functional was that in minimizing J the final position of the missiles would go to either target A or target B. The reason for this is that the additional missile term goes to zero when $y_{\text{missile final}} = y_{\text{target}}$. However the addition of a weight factor β was required in order to improve the precision in the missile reaching the targets. Larger values for the weight factor would allow the missiles to get closer to the target position, but the missiles would still not reach the actual target position. There was also an upper limit on the weight factor, and using values too large for the problem parameters would cause the solver to no longer allow convergence of the missile solutions to the correct targets, with extreme cases resulting in both missiles attempting to reach the same target. Properly chosen values for β did show improved precision in the missile reaching the correct target, but since a positional error did still exist, no attempt at proving the conditions of optimality being met were performed on this method.

6.3 A Better Designer Function

Reconstructing the chosen $\mathcal{F}(\mathbf{x})$ was able to eliminate the positional errors between the final endpoints for the missiles and the target locations. By adding another curve that maps the target endpoints introduces an additional event constraint that must be met in order for there to be a valid solution. This gave the following Designer Function, $\mathcal{F}_2(\mathbf{x})$,

$$\mathcal{F}_2(\mathbf{x}_1) = \begin{bmatrix} x_{1\,f} - b \\ y_{1\,f} \\ (x_{1\,f} - b)^2 + (y_{1\,f} - 0.5)^2 - (0.5 - \delta)^2 \\ (1 - y_{1\,f})(y_{1\,f}) \end{bmatrix} \tag{6.7}$$

and

$$\mathcal{F}_2(\mathbf{x}_2) = \begin{bmatrix} x_{2f} - b \\ y_{2f} \\ (x_{2f} - b)^2 + (y_{2f} - 0.5)^2 - (0.5 - \delta)^2 \\ (1 - y_{2f})(y_{2f}) \end{bmatrix} \tag{6.8}$$

where

$$\begin{matrix} e^L \\ \begin{bmatrix} 0 \\ 0 \\ 0 \\ 0 \end{bmatrix} \end{matrix} \quad \leq \quad \mathcal{F}_2(\mathbf{x}) \quad \leq \quad \begin{matrix} e^U \\ \begin{bmatrix} 0 \\ 1 \\ \infty \\ 0 \end{bmatrix} \end{matrix}$$

$$\leq \quad \mathcal{F}_2(\mathbf{x}_i) \quad \leq$$

The graphical representation of this $\mathcal{F}_2(\mathbf{x})$ is seen in Figure 6.2a. A curve of

$$(1 - y_{\text{missile}})(y_{\text{missile}}) = x$$

is used in addition to the line segment at x= 2 with the exclusion circle. The intersection of the three different curves results in the targets A and B being the only allowed endpoints for the missiles (Figure 6.2b). With the path constraint preventing the missiles from going to the same target because of the minimum separation distance one missile will go to target A and the other Target B. Since the individual curves are all allowed ending regions the resulting intersection does not possess the problem solution issues of looking at the target endpoints as disparate points in space. The logical connective of each entry in $\mathcal{F}(\mathbf{x})$, $(f_1 \wedge f_2 \wedge \ldots \wedge f_n)$, represents the continuous hypercurve that maps the disparate target endpoints into a continuous set. This allows the endpoints to be unique through the intersection of each f_i while also allowing the continuously differentiable nature that is required in a continuous calculus based solution. With the forced missile separation of the path constraint the exclusivity that is required for a target selection is met.

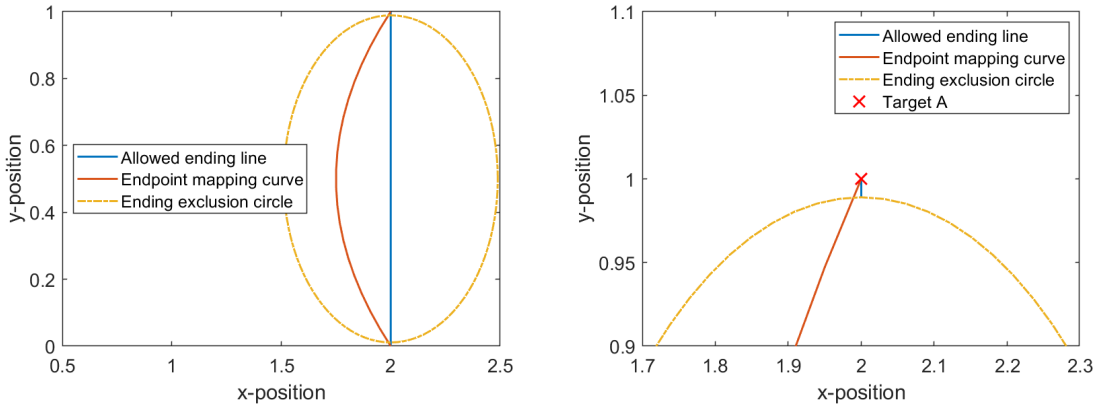

(a) (b)

Figure 6.2. (a) Missile Endpoint Functions. (b) Missile Endpoint Functions Zoomed in at Target A

Analysis of $\mathcal{F}_2(\mathbf{x})$ shows that it meets the requirements stated by Equations (6.1) - (6.2). The partials of $\mathcal{F}_2$ with respect to x_{if} do not result in a zero vector, instead resulting in,

$$\frac{\partial \mathcal{F}_2(\boldsymbol{x}_i)}{\partial x_{if}} = \begin{bmatrix} 1 \\ 0 \\ 2x_{if} \\ 0 \end{bmatrix} \quad \text{and} \quad \frac{\partial \mathcal{F}_2(\boldsymbol{x}_i)}{\partial y_{if}} = \begin{bmatrix} 0 \\ 1 \\ 2y_{if} \\ 1 - 2y_{if} \end{bmatrix}. \tag{6.9}$$

This prevents any numerical or mathematical inconsistencies with Pontryagin's Principle from arising due to the chosen Designer Function. Since the KKT conditions for the event multipliers, Equation (6.10), clearly show that some ν values are free, having a zero vector for a partial of $\mathcal{F}(\mathbf{x}_i)$ allows for possible issues to arise in the numerical solution construction.

$$\boldsymbol{\nu}_i \quad \begin{cases} \leq 0, & \text{if} \quad \mathcal{F}(\boldsymbol{x}) = e^L, \\ = 0, & \text{if} \quad e^L < \mathcal{F}(\boldsymbol{x}) \leq e^U, \\ \geq 0, & \text{if} \quad \mathcal{F}(\boldsymbol{x}) = e^U \\ \text{free}, & \text{if} \quad e^L = e^U \end{cases} \tag{6.10}$$

The Endpoint Lagrangian was constructed according to Equation (6.11). Since the final velocity is unconstrained the values of $\lambda(t_f)$ corresponding to angle and speed are zero. Constraints have been placed upon $x_i(t_f), y_i(t_f)$ the corresponding final costate values have final values allowed according to the terminal transversality of the Endpoint Lagrangian, Equation (6.11).

$$\bar{E}_{DSGN} = t_f + \nu_I^T \mathcal{F}(x_1) + \nu_{II}^T \mathcal{F}(x_2) \tag{6.11}$$

$$\boldsymbol{\lambda}(t_f) = \frac{\partial \bar{E}}{\partial \boldsymbol{x}_f} = \nu_I^T \frac{\partial \mathcal{F}(\boldsymbol{x_1})}{\partial \boldsymbol{x}_f} + \nu_{II}^T \frac{\partial \mathcal{F}(\boldsymbol{x_2})}{\partial \boldsymbol{x}_f} \tag{6.12}$$

$$\boldsymbol{\lambda}(t_f) = \begin{bmatrix} \nu_1 + 2\nu_3 x_{1f} \\ \nu_2 + 2\nu_3 y_{1f} + \nu_4(1 - 2y_{1f}) \\ 0 \\ 0 \\ \nu_5 + 2\nu_7 x_{2f} \\ \nu_6 + 2\nu_7 y_{2f} + \nu_8(1 - 2y_{2f}) \\ 0 \\ 0 \end{bmatrix} = \begin{bmatrix} \lambda_{x_1}(t_f) \\ \lambda_{y_1}(t_f) \\ \lambda_{V_1}(t_f) \\ \lambda_{\theta_1}(t_f) \\ \lambda_{x_2}(t_f) \\ \lambda_{y_2}(t_f) \\ \lambda_{V_2}(t_f) \\ \lambda_{\theta_2}(t_f) \end{bmatrix} \tag{6.13}$$

The HMC and the Hamiltonian Evolution remain unchanged from the system-of-systems approach at a constant $H(t) = -1$ with an allowed discontinuity at the activation of the separation constraint covariable μ_R.

6.4 Solution Using Designer Function 2

The DIDO provided solution to the target selection and trajectory optimization for the missile target pair using $\mathcal{F}_2(x)$ matched the target selection seen in the baseline approach from the system-of-systems shown in chapter 5 with the same time of flight of $t_f = 2.693$. Because the Designer Function does not tell the missiles what target to go to and DIDO's solutions are guess free [22], utilizing this method provides both a target selection and

trajectory optimization in one step. Moreover, because no guess was made by the user it may be concluded that the result was not a product of a user's "lucky" input.

The graph of the missile trajectories and the separation and position at closest approach matched what was observed with the system-of-system's baseline when compared together in Figure 6.3. The standoff distance for the missiles using the Designer Function approach was maintained, and the missiles reached the minimum separation distance at $t = 0.710$, just as in the solution from Chapter 5 following the system-of-systems approach.

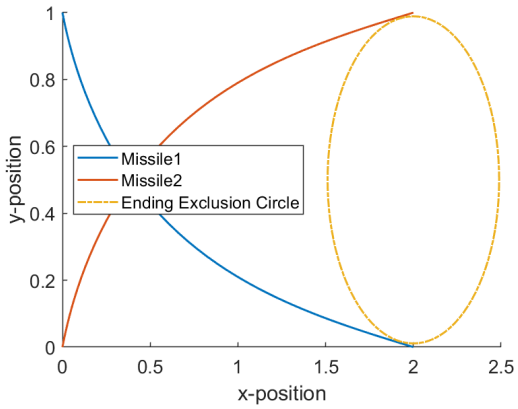

(a) $\mathcal{F}_2(x)$ Based Missile Trajectories

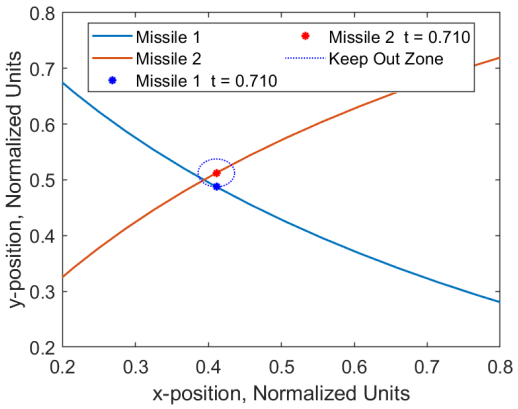

(b) $\mathcal{F}_2(x)$ Based Separation and Position

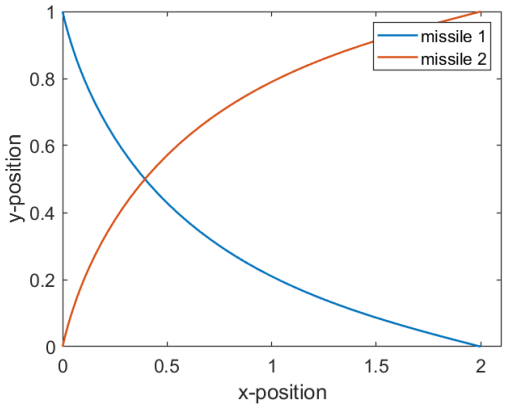

(c) System of Systems Missile Trajectories

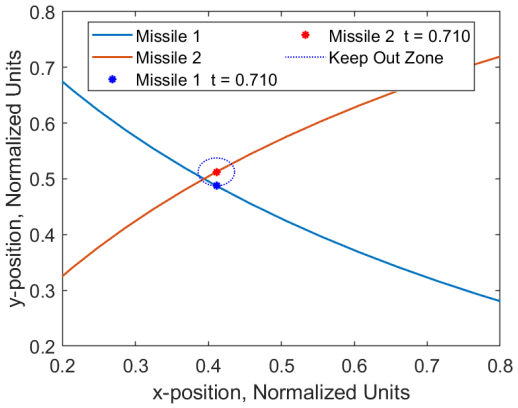

(d) System of Systems Separation and Position

Figure 6.3. Comparison of the Designer Function Trajectories and Closest Approach with Chapter 5's Trajectory and Closest Approach.

The trajectory solution using the proper $\mathcal{F}_2(x)$ matches theory as seen in Figure 6.4. The costate λ_y shows a sharp change at $t = 0.710$ when the Figures 6.4c and 6.4d. This is consistent with the adjoint equations due to $\dot{\lambda}_{y_i}$ being dependent on the μ_R. The covariables corresponding to the control inputs are consistent with the KKT conditions, showing a constant zero value since the control inputs never reach a maximum or minimum value (Figures 6.4e-6.4f).

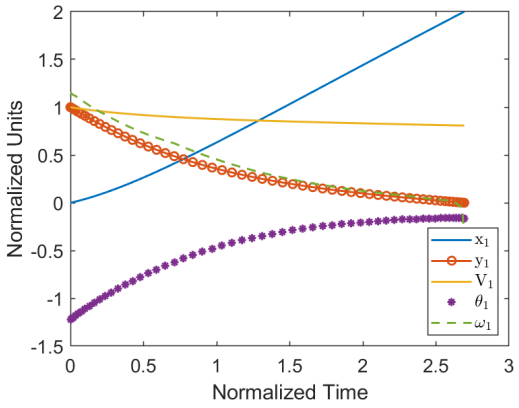

(a) States and Control

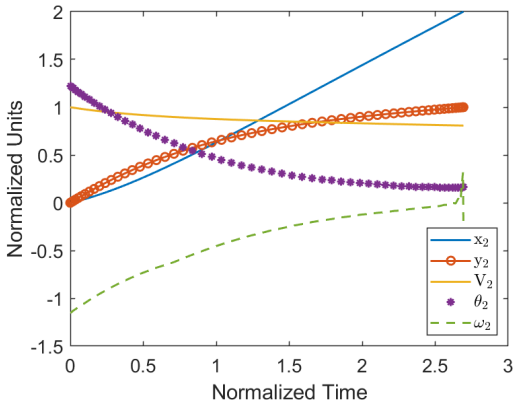

(b) States and Control

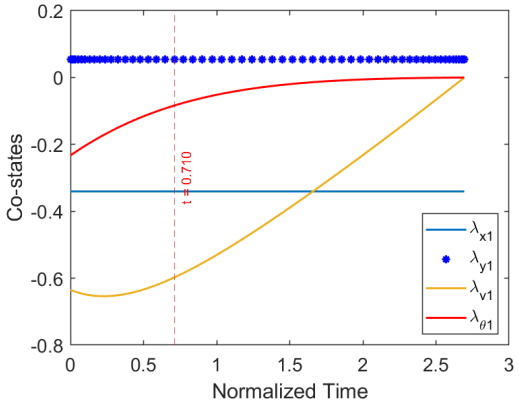

(c) Costates

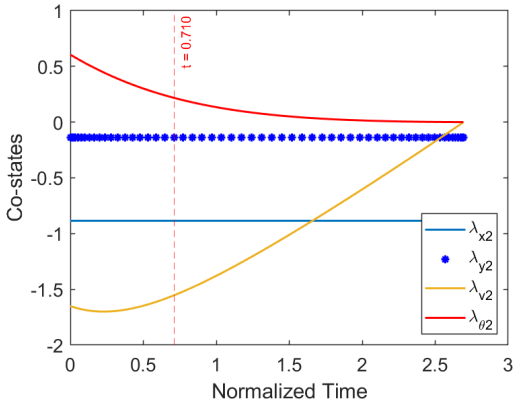

(d) Costates

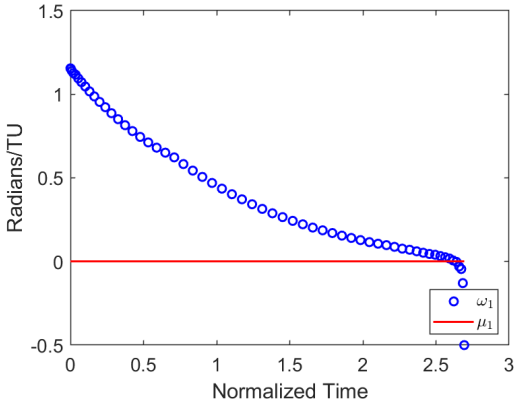

(e) Control and Covariable

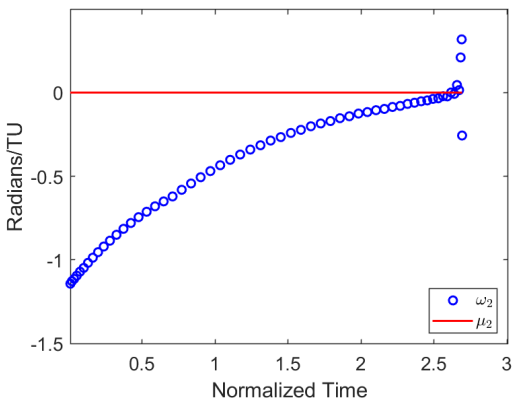

(f) Control and Covariable

Figure 6.4. Graphs of Optimality Conditions Left: Missile 1. Right: Missile 2.

The HMC and Hamiltonian Evolution conditions are also met referring to Figure 6.5a. The missile separation also does not go below the minimum distance R, with the covariable μ_R showing activation at the time the missiles reach the minimum distance R (Figures 6.5b-6.5c).

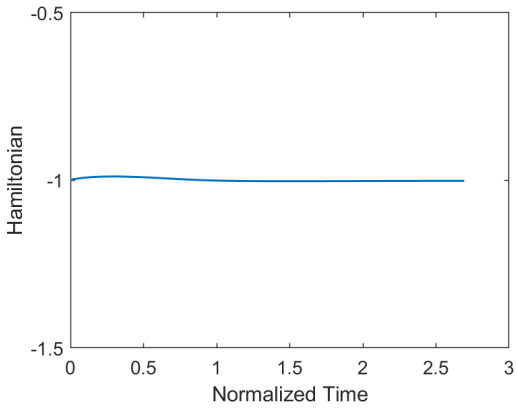

(a) Hamiltonian

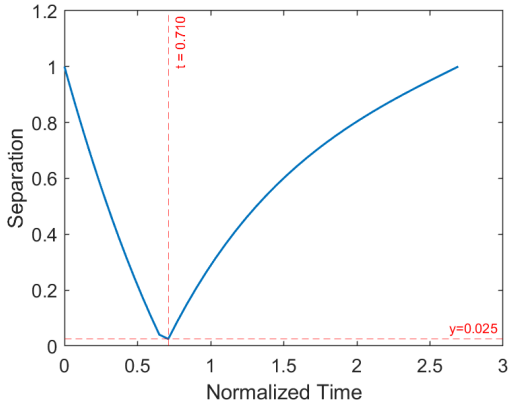

(b) Missile Separation

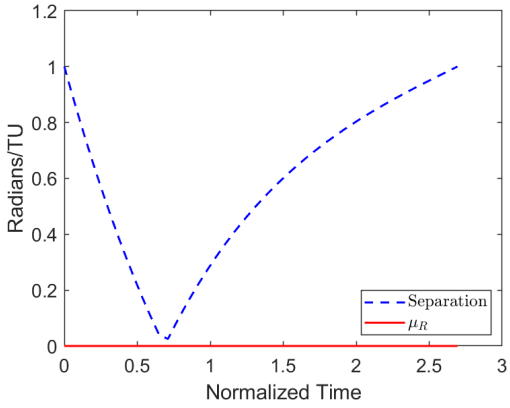

(c) Separation and μ_R

Figure 6.5. $\mathcal{F}(x)$ Based Solution's Hamiltonian, Separation and Separation Covariable μ_R.

6.5 Comparison to Lead and Follow-on Approach

Analysis for t_f for larger separation distances R between the missiles was performed. In all cases the trajectory solutions met the conditions for optimality, while choosing the correct

target assignment and maintaining the separation distance and the *XOR* condition for final targets.

Looking at the values of t_f for the different R values showed that larger missile separation required a longer missile flight time to reach the targets. This is consistent with maneuvering making the missiles both travel a longer distance as well as have reduced speed due to the induced drag from steering. Comparing these values of t_f to those of the follow-on missile scenarios of chapter 4 shows interesting results. In all cases the Designer Function approach resulted in faster time on target for the missiles. While the difference was small for the case of $R = 0.025$ the time difference quickly increase as R got larger as is seen in Table 6.1.

Table 6.1. Final Time Comparison Between Designer Function and Lead and Follow-on Approach

R	Designer Function t_f	Follow-on t_f	Δt_f
0.025	2.6932	2.6942	0.001
0.050	2.7087	2.7312	0.0225
0.075	2.7336	2.7948	0.0612
0.100	2.7704	2.8674	0.097

6.6 Chapter Summary

The utilization of a Designer Function allows for the simultaneous target selection and trajectory optimization. Comparisons with the baseline system-of-systems model of Chapter 5 show that the correct target selection is chosen despite no assignment information being given to the solver. Verification of optimality theory with the trajectory solutions demonstrated that this was consistent with Pontryagin's Principle for being an optimal solution. While the chosen Designer Function works for this OCP, that is not to say that other possible ways to construct the Designer Function that produces correct solutions. In fact, this concept should be explored as part of future work.

THIS PAGE INTENTIONALLY LEFT BLANK

CHAPTER 7:
Conclusions and Future Work

In this work four methods for a missile-target selection problem were analyzed. The problem setup was that of two simple glide bodies in a 2D cross-range and down-range with the targets A and B. The goal was to solve for which missile goes to which target with both simultaneous time of arrival and minimum time of flight for the missiles. The first method was a simple enumeration method over the possible missile-target pairings as is needed for a LSAP. The second was an enumeration method of a lead and follow-on missile setup, with collision avoidance in the follow-on missile's solution. This resulted in a LBAP format that could not ensure simultaneous time of arrival. The third was an enumeration of a system-of-systems approach to the missile trajectory solutions that allowed for both simultaneous time of arrival and missile collision avoidance. The fourth was a Designer Function approach that removed the inner and outer loop enumeration architecture and allowed the assignment optimization problem trajectory optimization problem to be solved simultaneously.

7.1 Conclusion

This thesis outlined that simple enumeration methods to produce a cost matrix for use in a target selection algorithm may result in possible collisions. This requires the problem architect to rewrite the problem in a system of systems approach to allow for the required collision avoidance and simultaneous time of arrival for the HGVs. It was demonstrated that a non-conjunctive constraint could be utilized as part of a time optimal control problem to solve a missile-target pairing through the use of a Designer Function that produced the same trajectory solutions as the system of systems model. The utilization of the Designer Function allowed each missile to "choose" their own target selection without explicit guidance on the missile-target pairing. The missile-missile avoidance provides the required XOR logic of a target selection problem. With the system coupling of the avoidance constraint to the Designer Function, the disparate target endpoints are mapped to a continuous function set that meets the requirements of a logically true conjunctive connectiveness for an OCP solution. In addition, the solution to the trajectory optimization and the target selection is done simultaneously with no required outer calls to solve the missile-target pairing when

using a properly formulated Designer Function.

The missile dynamics were that of a simplified toy model. This does not invalidate the solutions and findings of this thesis. In fact, using simple models allowed for the discovery of some unique features with the Designer Function approach. More complex and realistic missile modeling would be working with dynamics that just expand upon the generic dynamics that were used here. The generic dynamics are actually the limiting case for the more realistic modeling, and also demonstrate that collision issues as well as the target selection from the Designer Function approach are not artifacts of particular system dynamics.

7.2 Future Work

Further work still needs to be done on the simultaneous target selection and trajectory optimization. Expansion of the number of missiles and targets and the requirements on the Designer Function should be investigated. It has been shown in [27] that improperly constructed Designer Functions can lead to the solver getting caught in a demonstrable local minima and this hurdle would need to be carefully considered in expansion of the problem scope. Some other attentive approached are given in [28] that demonstrate avoidance of local minima in a solution space, as well as demonstrating that there is not one form of Designer Function that can result in a correct target assignment solution.

Additionally the dynamics of the HGV should be expanded to look into a 3-dimensional problem, (for example a spherical rotating earth model that has been demonstrated for a glide vehicle in [29]), compared to this thesis' 2-D formulation. In doing so additional considerations should be considered on the missile dynamics, such as lift and drag profiles, thermal heating constraints etc., to not under-determine the system and its solution space. Also, real world problem formulations would not be limited to looking at symmetric flight dynamics and missile-target pathing. This asymmetry could be investigated in the future.

List of References

[1] A. Andersen, K. Pavlikov, and T. Toffolo, "Weapon-target assignment problem: Exact and approximate solution algorithms," *Annals of Operations Research*, vol. 312, pp. 581–606, May 2022.

[2] S. Matlin, "A review of the literature on the missile-allocation problem," *Operations Research*, vol. 18, no. 2, pp. 334–373, 1970. Available: http://www.jstor.org/stable/168691

[3] G. G. den Broeder, R. E. Ellison, and L. Emerling, "On optimum target assignments," *Operations Research*, vol. 7, no. 3, pp. 322–326, 1959. Available: http://www.jstor.org/stable/166837

[4] R. K. Ahuja, A. Kumar, K. C. Jha, and J. B. Orlin, "Exact and heuristic algorithms for the weapon-target assignment problem," *Operations Research*, vol. 55, no. 6, pp. 1136–1146, 2007. Available: http://www.jstor.org/stable/25147151

[5] Z.-J. Lee, S.-F. Su, and C.-Y. Lee, "Efficiently solving general weapon-target assignment problem by genetic algorithms with greedy eugenics," *IEEE Transactions on Systems, Man and Cybernetics. Part B, Cybernetics*, vol. 33, no. 1, pp. 113–121, 2003.

[6] X. Lu, H. Di, Z. Jia, and X. Zhang, "Optimal weapon target assignment based on improved qpso algorithm," in *2019 International Conference on Information Technology and Computer Application (ITCA)*, 2019, pp. 217–220.

[7] C. Liu, C. Zhang, and F. Xiong, "Multistage cooperative trajectory planning for multimissile formation via bi-level sequential convex programming," *IEEE Access*, vol. 8, pp. 22 834–22 853, 2020.

[8] Y. Wang, S. Dong, L. Ou, and L. Liu, "Cooperative control of multi-missile systems," *IET Control Theory & Applications*, vol. 9, no. 3, pp. 441–446, 2015. Available: https://onlinelibrary.wiley.com/doi/abs/10.1049/iet-cta.2014.0361

[9] J. McFarland, "The development of hypersonic weapons in the US, China and Russia: An incipient arms race," *The RUSI journal*, vol. 168, no. 1-2, pp. 10–18, 2023.

[10] M. McWhinney, "The risks of hypersonic weapons," *Project Ploughshares*, Dec. 3 2020 [Online], Accessed Oct. 8 2023. Available: https://www.ploughshares.ca/reports/the-risks-of-hypersonic-weapons

[11] K. W. Iliff and M. F. Shafer, "A comparison of hypersonic vehicle flight and prediction results." Legacy CDMS: NASA, 1995.

[12] *The U.S. Army's Long-Range Hypersonic Weapon (LRHW)*. Congressional Research Service, 2023. Available: https://crsreports.congress.gov/product/pdf/IF/IF11991

[13] R. Parlato, "1st multi-domain task force deploys the Army's first long-range hypersonic weapon system," *www.army.mil*, 2023. Available: https://www.army.mil/article/265349/1st_multi_domain_task_force_deploys_the_armys_first_long_range_hypersonic_weapon_system

[14] *Hypersonic Weapons: Background and Issues for Congress*. Congressional Research Service, 2023. Available: https://crsreports.congress.gov/product/pdf/R/R45811

[15] J. Trevithick, "Navy wants triple-packed hypersonic missile modules on its stealthy Zumwalt destroyers," *The Drive*, Mar. 19 2021 [Online], Accessed Oct. 8 2023. Available: https://www.thedrive.com/the-war-zone/39867/navy-wants-triple-packed-hypersonic-missile-modules-on-its-stealthy-zumwalt-destroyers

[16] I. M. Ross, *A Primer on Pontryagin's Principle in Optimal Control*, 2nd ed. Carmel, CA: Collegiate Publishers, 2015.

[17] E. Mendelson, *Introduction to Mathematical Logic*, 3rd ed. (The Wadsworth Brooks/Cole mathematics series). Monterey, CA: Wadsworth Brooks/Cole Advanced Books Software, 1987.

[18] E. VonWeller, "Boolean XOR endpoint constraints in continuous-time optimal control problems," M.S. thesis, Dept. of Mech. and Aerosp. Eng., Naval Postgraduate School, Monterey, CA, USA, 2020.

[19] L. Pontryagin, *Mathematical Theory of Optimal Processes*. Routledge, 2018.

[20] I. M. Ross, "Enhancements to the DIDO optimal control toolbox," *arXiv.org*, 2020. Available: http://doi.org/10.48550/arxiv.2004.13112

[21] I. Sutskever, J. Martens, G. Dahl, and G. Hinton, "On the importance of initialization and momentum in deep learning," in *Proceedings of the 30th International Conference on Machine Learning* (Proceedings of Machine Learning Research), S. Dasgupta and D. McAllester, Eds., no. 3. Atlanta, Georgia, USA: PMLR, 17–19 Jun 2013, vol. 28, pp. 1139–1147. Available: https://proceedings.mlr.press/v28/sutskever13.html

[22] Q. Gong and I. M. Ross, "Guess-free trajectory optimization," in *AIAA/AAS Astrodynamics Specialist Conference and Exhibit*, Honolulu, HI, August 18-21, 2008. Available: https://arc.aiaa.org/doi/pdf/10.2514/6.2008-6273

[23] J. A. Englander and B. Conway, "An automated solution of the low-thrust interplanetary trajectory problem," *Journal of Guidance, Control, and Dynamics*, vol. 40, no. 1, pp. 15–27, 2017.

[24] B. J. Wall and B. A. Conway, "Genetic algorithms applied to the solution of hybrid optimal control problems in astrodynamics," *Journal of Global Optimization*, vol. 44, no. 4, pp. 493–508, 2009.

[25] R. E. Burkard, M. Dell'Amico, and S. Martello, *Assignment Problems*, Rev. Reprint ed. Philadelphia, Pa: Society for Industrial and Applied Mathematics, 2012.

[26] M. Karpenko, R. J. Proulx, and M. Zepeda, "Bipartite graph learning for autonomous task-to-sensor optimization," Naval Postgraduate School (U.S.), Monterey, CA, Tech. Rep. NPS-MAE-22-002, 2022.

[27] M. Zepeda and M. Karpenko, "Autonomous landing site selection of a lunar lander." Big Sky, MT: AIAA/AAS Astrodynamics Specialist Conference and Exhibit, 13-17 August 2023.

[28] M. Karpenko, M. Zepeda, J. King, and R. J. Proulx, "Bilevel hypersonic target assignment optimization," Naval Postgraduate School (U.S.), Monterey, CA, Tech. Rep. NPS-MAE-23-007R, 2023.

[29] K. P. Bollino, "High-fidelity real-time trajectory optimization for reusable launch vehicles," PhD thesis, Dept. of Mech. and Aerosp. Eng., Naval Postgraduate School, Monterey, CA, USA, 2006.

THIS PAGE INTENTIONALLY LEFT BLANK

Initial Distribution List

1. Defense Technical Information Center
   Ft. Belvoir, Virginia

2. Dudley Knox Library
   Naval Postgraduate School
   Monterey, California